Open Access

Recent Progress in Materials

LIDSEN Publishing Inc.

Original Research

Obtaining of WC–Co- and WC–TiC–Co-Based Ultradispersive Alloys Modified with B_4C–TiB_2 Quasieutetic

Otar Tsagareishvili [1], Archil Mikeladze [1], Roin Chedia [1, 2], Tamaz Batsikadze [3], Levan Chkhartishvili [1, 4, *]

1. Semiconducting and Powder Composite Materials Laboratory, Ferdinand Tavadze Metallurgy and Materials Science Institute, 8b Elizbar Mindeli Street, Tbilisi, 0186, Georgia; E-Mails: t_otari@hotmail.com; mikeladze.archil@gmail.com; chediageo@yahoo.com; levanchkhartishvili@gtu.ge
2. Petre Melikishvili Institute of Physical and Organic Chemistry, Ivane Javakhishvili Tbilisi State University, 31a Anna Politkovskaya Street, Tbilisi, 0186, Georgia
3. Structural and Physical-Chemical Properties Research Laboratory, Ferdinand Tavadze Metallurgy and Materials Science Institute, 8b Elizbar Mindeli Street, Tbilisi, 0186, Georgia; E-Mail: tamaz4l4fx@gmail.com
4. Engineering Physics Department, Georgian Technical University, 77 Merab Kostava Avenue, Tbilisi, 0160, Georgia

* **Correspondence:** Levan Chkhartishvili; E-Mail: levanchkhartishvili@gtu.ge

Academic Editor: Ali Abdul-Aziz

Special Issue: Ceramic Matrix Composites: Performance Evaluation and Application

Recent Progress in Materials
2024, volume 6, issue 3
doi:10.21926/rpm.2403021

Received: March 21, 2024
Accepted: August 13, 2024
Published: August 26, 2024

Abstract

Tungsten carbide WC-based materials characterized by high hardness and wear resistance have long been widely used in manufacturing cutting and mining tools. They are alloyed or modified with different ceramic phases to improve operational characteristics further. There are obtained the hard tungsten carbide–cobalt WC–Co and tungsten carbide–titanium carbide–cobalt WC–TiC–Co metal-ceramic alloys ultradispersed powders modified with quasieutectic ceramic alloy B_4C–30wt.%TiB_2 and complex samples compacted from them. The

quasieutectic alloy used as a modifier has almost as high hardness as pure boron carbide. Still, it is characterized by higher electrical and thermal conductivities of several orders of magnitude. Two groups of hard alloys modified with B_4C–30wt.%TiB_2 were studied: BK8 grade WC–Co and T30K4 and T15K6 grades WC–TiC–Co. Metal-ceramic composite powders of different concentrations are obtained by chemical synthesis and mechanical dispersion in an attritor. The particle size of chemically synthesized composite powders is ≤0.3 μm, and those obtained by mechanical dispersion are ≤0.8 μm. SPS (Spark-Plasma Sintering) and HTS (High-Temperature Sintering) methods compact these powder materials. Phase composition of the obtained materials, distribution of chemical elements in them, and structural features are investigated by the XRD (X-Ray Diffraction) method and EDX (Energy Dispersive (micro)X-ray) spectrometry and optical and electron microscopies, respectively. Key physical-mechanical characteristics of the received samples, such as hardness, microhardness, and bending strength, are studied. Ultradispersed (≤0.8 μm) metal-ceramic alloys of the WC–Co–B_4C–TiB_2 system with interesting characteristics have been obtained using the WC–Co hard alloy of BK8 grade as the matrix. A SPS-compacted sample's hardness, microhardness, and bending strength are 93.0 HRA, 3350 kgf/mm^2, and 100 kgf/mm^2, respectively. Among the WC–TiC–Co system materials, the T15K6 grade-based hard alloy modified with 15wt.%(B_4C–30wt.%TiB_2) has the best characteristics with hardness, microhardness, and bending strength of 91.5 HRA, 2900, and 117 kgf/mm^2, respectively. A preliminary study of the problem of environmentally safe utilization of tungsten-containing scrap and tungsten waste is also carried out as part of the work. In particular, the tungsten heater waste is treated in hydrogen peroxide, and by adding specific liquid components to the tungsten-containing proper solution in a single utilization–synthesis cycle, the target product – ultradispersed WC–Co hard alloy is obtained.

Keywords
Hard composite; ceramic matrix; metallic binder; quasistatic modifier; ultradispersive state; physical-mechanical characteristics

1. Introduction

The rapid development of new technologies leads to increasing demands for functional materials (for an example, see the recent review [1]). The creation of hard materials operating in aggressive environments and at high temperatures deserves particular interest [2]. Among them are tungsten carbide-based metal-ceramic materials with high hardness and wear resistance. For decades, they have been widely used to make cutting and mining tools for hard metallic materials. Nevertheless, in the recent literature there are presented a number of studies devoted to the further improving their operational characteristics.

Tungsten carbide grain size is the most important parameter for adjusting such alloys' hardness/strength ratio. The smaller the grain size, the greater the hardness at a given composition of the cementing phase. The ratios between the system components' quantities determine the composite material's physical-mechanical and operational characteristics. Suppose the composition of the alloy is fixed. In that case, the important factors that lead to the improvement of its

mechanical characteristics are porosity, average particle size, structure uniformity, and purity of the initial powders. Further increase in hardness is also possible by modifying material with various metal carbide phases.

It is why metal carbide-based hard alloys are sometimes classified according to the content of the carbide-forming metals that are the main components of the material. Tungsten, titanium, tantalum, and completely tungsten-free hard alloys are known. Cobalt and nickel are also mainly used for cementing elements as chemically neutral materials with respect to carbon and carbide phases present in the composite since cobalt itself does not form carbides.

The paper aims to increase the hardness and wear resistance of tungsten carbide-based metal-ceramic alloys in two main directions: (1) Obtaining WC–Co and WC–TiC–Co alloys in the ultradispersed state by chemical synthesis from liquid charges and (2) Modifying them with ultradispersed superhard B_4C–30wt.%TiB_2 quasieutectic alloy. In addition, the research involves investigating the development of environmentally safe utilization processes of tungsten-bearing scrap and tungsten waste and determining the possibilities of synthesizing tungsten-containing hard alloys from the materials obtained in this way.

These objectives require relevant reviews of representative data on B–C–W–Ti–Co systems, in general, and B_4C–W composites, in particular, and tungsten scrap and waste utilization methods. They are given below in Subsections 1.1, 1.2, and 1.3, respectively.

1.1 B–C–W–Ti–Co Systems

Usually, techniques use such solid metal ceramic alloys, the essential components of which are refractory metal carbides, for example, tungsten WC, titanium TiC, and tantalum TaC carbides, and metal binders are mainly cobalt, nickel, and their or other metals alloys. These alloys contain 70–97% hard melting carbides. They are characterized by high hardness of 86–92 HRA, red- (800–1000°C), and abrasion resistances. The higher the amount of metal binder in the alloy, the lower its hardness and wear resistance and the higher the strength.

Hard alloys are conventionally divided into four groups:

(1) Single-carbide tungsten composite WC–Co consists of tungsten carbide and cobalt and is sometimes marked as BK plus a number indicating the cobalt wt.% content in the alloy. For example, BK8 designates that Co and WC are 8 and 92wt.%, respectively.

(2) Two-carbide titanium–tungsten composite WC–TiC–Co consists of tungsten carbide as matrix, titanium carbide, and cobalt as components. Sometimes, this grade is marked as TK and numbers. The numbers after T and K show the contents of titanium carbide and cobalt in wt.%, respectively. The rest of the alloy, again, is tungsten carbide.

(3) Titanium, tantalum, and tungsten alloys WC–TiC–TaC–Co contain tungsten carbide as matrix, titanium and tantalum carbides as components, and metallic cobalt as binder.

(4) Tungsten-free alloys usually consist of titanium carbide, carbonitride, and nickel Ni or nickel–molybdenum NiMo alloy. TiC–NiMo and TiC–TiN–NiMo alloys are sometimes assigned TH and KTH grades, respectively [3].

Some reviews on B–C–W–Ti–Co systems are available. For example, the results of sintering nanocrystalline WC–Co powders and technologies for producing nanosized WC powders were examined in [4]. It was discussed that the critical challenge to producing bulk nanocrystalline cemented tungsten carbide materials is controlling the rapid grain growth during the early sintering

stage. The review [5] presented and discussed the cemented carbide phase diagrams of W–C–M with M = (Co, Fe, Ni, FeNi, FeAl, CoFeNi, Cr, and CrFe). Production processes for fine powders of tungsten, tungsten carbide, and WC–Co and sintering methods for nanosized WC–Co hard metals were also reviewed in [6]. It was established that, regardless of the process, the mandatory requirements for the production of fine hard metals are (i) purity of starting materials, (ii) precise compliance with the process procedure, and (iii) careful control at all production stages, which exclude unwanted phases and defects in the structure. The paper [7] aimed to present a review on the machining of tungsten carbide–cobalt composite material, as machining of the WC–Co materials is difficult and with conventional machining processes results in poor surface finish, low material removal rate, high cost, etc. Among all non-conventional machining processes, thermal energy-based processes, such as wire EDM (Electrical Discharge Machining), are more frequently used for these materials. The machining of WC–Co is also affected by cobalt content, grain size, and the presence of other carbides.

Historical review [8] of the development of CVD (Chemical Vapor Deposition) and PVD (Physical Vapor Deposition) processes showed a continuous improvement of successful coating materials through adjustments of the chemical composition and the coating architecture. Cutting tools are an excellent example of how coated product development is traced methodologically using a holistic view of the application. A comprehensive review [9] on progress in developing high-performance WC-based composites included the categories of composites, the strategy to enhance their properties, and their typical applications. The review [10] discussed various WC grain growth modes and details of grain growth inhibition and reported on the influences of grain growth inhibitors on the microstructure and properties of hard metals. Recognized mechanisms of grain growth inhibition, based on segregating thin films of carbide phases at WC/Co grain boundaries, were summarized.

The study [11] summarized the knowledge of the impacts of different binders, partial or total substitution of the traditional cobalt binder, highlighting the influences of metal, intermetallic compound, and ceramic (metal oxide) binders on the sintering behavior as well as mechanical properties of WC-based alloys. It was concluded that the alternative for cobalt in tungsten carbide cemented carbide is economically and technically feasible. In the work [12], various approaches to machine hard materials, like tungsten carbide WC and its composite WC–Co by EDM techniques, were discussed, as well as its operational parameters and their consequences on such machining characteristics. In the review [13], the selected cemented carbide and cermet microstructures were presented. Cemented carbides were divided into four groups based on microstructure and chemistry: WC morphology and chemistry, cubic carbide containing ones and cermets, functionally graded, and binder designed.

1.1.1 WC–Co System

Tungsten carbide compound produced by powder metallurgy methods, which are widely used to develop the tool materials necessary for high-speed processing, consists of carbide particles – usually tungsten carbide WC itself and a relatively soft metal binder. There are known the hundreds of WC-based alloys, most of which use cobalt Co, nickel Ni, and chromium Cr as binders and other binders with various metallic and non-metallic additives.

Tungsten carbide WC is characterized by high hardness at room temperature, primarily maintained at high temperatures. However, it lacks high-temperature strength, an essential property for cutting tools. Metal carbide binders are used to keep the high hardness of tungsten carbide while increasing its toughness. The composite obtained in this way should have a much higher hardness than high-speed steel and a higher rate of service life.

Microstructure and mechanical properties of WC–10wt.%Co cemented carbides fabricated by the SPS (Spark-Plasma Sintering) process were investigated in [14]. Nanocrystalline precursor powders were prepared by spray drying from a solution containing ammonia metatungstate and cobalt nitrate. This was followed by reduction and carbonation into nanocrystalline WC–Co composite powders by a mechanochemical process. The nanocrystalline WC–10wt.%Co powders were consolidated by SPS at temperatures ranging from 900–1100°C and under 50–100 MPa pressures. It was found that cemented carbide's hardness depends on WC's density and grain size. The fracture toughness of cemented carbides decreases rapidly when the liquid Co phase is formed during sintering. Using the PCAS (Pulsed Current Activated Sintering) method, binderless WC and WC–Co were densified with 8, 10, and 12wt.% Co hard materials were accomplished [15] using ultrafine powders of WC and WC–Co. Nearly fully dense (with a relative density of up to 99.2%) WC and WC–Co were obtained with 60 MPa pressure and electric current application within 2 min. The average grain size of WC produced was about 380 nm. The near-nanocrystalline WC–10wt.%Co alloys were prepared [16] by SPS using sub-micron WC/nano-Co and sub-micron WC/micron-Co as the raw powders. Compared with the bulk prepared using the sub-micron mixed powders, the sintered bulk with pre-treatment of ball-milling has high density, hardness of 94.5 HRA, and fracture toughness of 13.5 MPa·$m^{1/2}$, respectively.

A rapid route for preparing WC–Co cemented carbides bulk, which integrated the synthesis of the composite powder by in situ reactions and subsequent consolidation in the SPS system, was proposed in [17]. The obtained WC–Co bulk had a homogeneous and fine-grained structure and a good combination of mechanical properties. Increasing the amount of metal binder in the WC–Co alloy decreases its hardness. The hardness of this material also depends on the size of the tungsten carbide particles: the hardness of the alloy decreases with the increase in the carbide grains size [18]. The literature describes [19, 20] the obtaining technology and properties of ultradispersed hard alloys WC–6wt.%Co and WC–10wt.%Co containing tantalum carbide. The hardness, bending strength and cracking coefficient are 93.5 and 93.0 kg/mm^2, 1670 and 1870 MPa, 11 and 16 MPa·$m^{1/2}$, respectively. It has been shown that adding 0.5–2% tantalum carbide TaC increases the hardness while the bending strength remains practically unchanged.

Cemented tungsten carbide with ultrafine grains can be prepared [21] via microwave sintering. In this way, the η-W_3Co_3C phase was formed on the sample surface. Extra carbon black was premixed. The maximum hardness and transverse rupture strength values are 93.2 HRA and 3396 MPa, respectively, when the carbon black content is 0.45%. The growth of WC grains mainly occurs during the early stage of microwave sintering due to the coalescence of grains. SPS and HIP (Hot Isostatic Pressing) were taken [22] as the representative methods of rapid and liquid-state sintering technologies to fabricate the WC–Co cemented carbides. The big difference in mechanical properties of the cemented carbides prepared by SPS and sinter-HIP depends on the configuration of WC and Co phases and the WC/Co orientation relationship resulting from the sintering technologies' intrinsic features. The chemical synthesis of tungsten carbide–cobalt WC–Co nanocomposite powders via a processing technique using all water-soluble precursors allowed [23]

commercial-scale production by a combination of molecularly mixed W-, Co-, and C-containing solutions into a complex inorganic polymeric powder precursor. Its conversion into W–Co–C–O powder intermediated by treatment at 500–600°C in an inert atmosphere was followed by treatment at a temperature <1000°C in nitrogen. The parts sintered and consolidated by liquid phase sintering technique had an excellent hardness of >93 HRA, with WC grains in the order of 200–300 nm. At the same time, Co was uniformly distributed on the WC grain boundaries. The presence of Co precipitates inside WC nanograins was also reported. In the work [24], different vacuum sintering temperatures (1250, 1300, 1350, and 1400°C) were studied to determine the optimal process parameters of nano-WC–15wt.%Co (as well as WC–15wt.%(Fe–Ni–Co) for comparison) hard metal alloys. The optimal sintering temperature was 1350°C for 1 h. The material showed an excellent contiguity of 0.42. Hardness was enhanced to 90.92 HRA. The transverse rupture strength increased to 2860 MPa. Moreover, flexural strength was 12.33 MPa·$m^{1/2}$.

The study [25] measured the thermal expansion and thermal conductivity of WC–Co material. The CTE (Coefficient of Thermal Expansion) of WC–Co was found to be intensely dependent on cobalt content. Grain size and microstructure had no apparent effects on CTE. In contrast, the thermal conductivity of WC–Co is affected by all the factors. Larger grain size and less cobalt lead to higher thermal conductivity. As the literature data on CTE values for cemented tungsten carbide alloys (WC–Co) containing products vary significantly, the work [26] was focused on true CTE of cemented tungsten carbide with different cobalt content and temperature in ranges of 3–20wt.% and 20–650°C, respectively. The relationship between CTE and temperature was linear, and the coefficients of the corresponding approximating functions for different cobalt content were calculated. With increasing the cobalt content, the value of CTE and the rate of its change with temperature enlarge linearly.

The SPS method was used [27] to produce bulk carbides from mixed WC–7.5wt.%nano-Co powders. Pressures ranging from 30 to 80 MPa were applied during sintering. The maximum hardness was found for the samples pressed at 80 MPa, which is ~1925 HV. The marked changes in porosity, hardness, and crack propagation showed that the sintering pressure considerably impacts the mechanical properties of cemented carbides. PPC (Pulse Plasma Compaction) was applied [28] to a series of WC–Co samples with varying sintering temperature, pressure, and initial particle size in order to study the mechanical and microstructural behavior. A high hardness of more than 2000 HV was achieved, while maximum fracture toughness of 15.3 MPa·$m^{1/2}$ was recorded in samples sintered at 1100°C and 100 MPa. While grain size showed an incremental pattern with increasing temperature, limiting those largely ensured that high mechanical properties were still possible. The effect of sintering pressure in the range of 60–100 MPa at the temperature kept constant was almost negligible. Inhomogeneous WC–(fine-WC–Co) cemented carbides with improved hardness and toughness were prepared [29] by adding fine WC using planetary ball milling combined with HIP technology. The inhomogeneous microstructure consisted of coarsened WC grains and WC–Co consisting of fine WC dispersoids and Co binder phase. The increase in temperature and the addition of fine WC enhanced the sintering process. The morphologies of the coarsened WC and the fine WC consisted of triangular and near-hexangular prisms, respectively. The prism-like coarsened WC crystals efficiently hindered crack propagation. The inhomogeneous WC–(fine-WC–Co) cemented carbides with 10wt.% fine WC, sintered at 1430°C for 40 min, provided the best combination of hardness and toughness.

The WC–6Co powders were fabricated [30] via hydrogen reduction and ball milling routes. In the case of milling, some multifaceted WC crystals contained multiple-step features, and the number of these multi-steps increased with milling time. No multi-steps occurred in the reduction case, and the plate-like WC crystals formed. These differences in the morphology of WC crystals might be ascribed to the shift from a 2D nucleation mechanism to a defect-assisted one. WC–6wt.%Co cemented carbide obtained from the hydrogen reduction route showed improved mechanical properties, a superior combination of hardness, fracture toughness, and strength compared to those obtained from the ball milling route. In work [31], a core–shell structured precursor was used to prepare WC–Co composite powders, and then the bulk materials were fabricated using the rapid HPS (Hot-Pressing Sintering) technique. The pure-phase composite powders with an average grain size of 80 nm were obtained in the short term at mild conditions. The as-prepared bulk sample exhibits a homogeneous microstructure and good mechanical properties. The WC–Co cemented carbides with 4–14wt.% Co content was fabricated [32] by SPS. The grain size of cemented carbide with different Co content was 220–380 nm. As the Co content increased, the density, fracture toughness, and flexural strength increased, but the hardness gradually decreased by ~1.6 GPa per 2wt.% increase in the Co content at 8wt.% Co. The optimal mechanical properties were: hardness of 19.87 GPa, fracture toughness of 12.27 MPa·$m^{1/2}$, and flexural strength of 1834 MPa.

Coarse-grained WC–Co cemented carbides with Co content varying from 3 to 12wt.% were fabricated [33] from composite powder prepared through a chemical coating method that cobalt encased on the surface of WC particles. Nanostructured cobalt coating exhibited a spherical shape with a particle size ranging from 200 to 400 nm, and the WC–Co composite powder represented a unique feature of WC particles encased by cobalt. With increasing Co content from 3 to 12wt.%, the gradual increase of WC grain size from 5.23 to 6.67 μm, fracture toughness from 24.66 to 28.83 MPa· $m^{1/2}$, and transverse rupture strength from 2367 to 2849 MPa of the WC–Co cemented carbides were resulted. The enhanced overall performance was attributed mainly to the WC's equilibrium shape caused by the cobalt's well-encasing on the WC grain. In the study [34], ultrafine tool materials were produced by SPS using three sets of WC–8wt.%Co nanopowders mixed by different methods. At a sintering temperature of 1250°C, cemented carbide sintered from the powder mixed by ultrasonic vibration method exhibited homogeneous microstructure, high relative density (99.1%), small average grain size (280 nm), and excellent mechanical properties (Vickers hardness of 18.8 GPa and flexural strength of 11.4 MPa·$m^{1/2}$). However, cemented carbide sintered from heavily ball-milled (for 24 h) powder showed increased grain coalescence and micro defects, as well as a lower relative density of 94.6%. Its hardness decreased to 17.7 GPa due to the decrease in relative density. Straight cracks along grain boundary became dominant, causing fracture toughness to decline to 10.5 MPa·$m^{1/2}$.

It has been shown [35] that the addition of 1–12wt.% vanadium carbide VC in the WC–6wt.%Co alloy slightly, no more than by 3%, increases the hardness of the material, but significantly (by 33–50%) improves its wear resistance, compared to unmodified WC–6wt.%Co. In addition, properties and characteristics of WC–6wt.%Co hard alloy separately modified with VC and rhenium carbide ReC were discussed. In particular, with the addition of ReC to 5wt.%, the wear efficiency of WC–6wt.%Co increases to 66.3%, and the tool's working resource rises to 35.0%. The work [36] proposed additive manufacturing technology for producing small dimensions and complex configuration details. It includes SLM (Selective Laser Melting), SEBM (Selective Electron Beam Melting), inkjet additive binder manufacturing, 3D gel printing, and melting. The main problems that arose during

the implementation of this method were discussed. It has been shown that product properties depend on the WC particle size and the amount of Co in the composite. Due to the uneven energy distribution, the microstructure of the samples obtained by SLM- and SEBM-methods is not uniform, so their properties are unstable. In addition, in the samples obtained by SLM, cobalt and carbon are burned due to the high energy density, and their losses occur. In this case, cracked and brittle samples are obtained, and if one reduces the energy density, then the cobalt cannot melt completely, and the samples turn out to be porous, etc. The use of each new material considers its chemical composition and grain size of the initial powder, which requires its preliminary study and determination of appropriate technological parameters for synthesis.

The WC–Co cemented carbides with the dual-grain structure were prepared [37] via in-situ carbothermic reduction of tungsten oxide WO_3, followed by liquid sintering in a single thermal cycle, utilizing carbon black, Co, WO_3, and coarse WC as raw powders. The carbothermic reduction of WO_3 was finished under 800°C, and microstructures of cemented carbide were composed of small WC grains with nearly round granular morphology and coarse WC grains with morphology of equilibrium triangle prism columns. Coarse WC grains were evenly encircled by small WC grains, showing an apparent dual-grain structure. Due to such structure, the material exhibited similar hardness to cemented carbides fabricated by the mixtures of fine WC, coarse WC, and Co powders. Fracture toughness was significantly improved because of crack deflection, transgranular fracture, and crack bridging. Cemented carbides with dual-grain structures showed good mechanical properties with Rockwell hardness of 89.8 HRA, transverse rupture strength of 3415 MPa, and fracture toughness of 13.5 MPa·$m^{1/2}$, respectively.

The effect of ultrafine WC on the macroscopic shrinkage behavior and microstructural evolution of coarse-grained WC–Co cemented carbides during sintering was studied in [38]. WC–Co composite powders containing a mixture of ultrafine (300 nm) and coarse (6.0 μm) WC powders were prepared using a novel sol–gel process. Ultrafine WC addition enhanced shrinkage in the composite powder compacts during solid-state sintering, while its influence on the densification process in liquid-phase sintering can be ignored. Ultrafine WC addition promoted the spreading of cobalt binder and the formation of WC–Co agglomerates in the initial sintering state. Ultrafine WC addition resulted in uniform densification in the solid-state sintering. Mechanisms of the enhanced shrinkage include the accelerated spreading of Co due to shortened diffusion distances, the increased surface diffusion velocity, and the activated sintering of the WC skeleton due to grain boundary sliding.

Impact toughness increases and hardness decreases with increasing Co content and average WC grains size, with some exceptions where impact toughness (and, consequently, cracking resistance) can be increased at the expense of hardness and thus wear resistance. According to the work results [39], the maximum strength limit is reached when the average grain size of WC varies from 1.4 to 5.3 μm and the amount of Co in the alloy is 6wt.%. The maximum compressive strength was achieved when the average grain size of WC changed from 1.4 to 1.7 μm. As for the bending strength limit practically does not change with further reduction of the average grain size. Work [40] presents the WC-based composites with various binder metal systems, such as WC–Co, WC–Ni, WC–CoNi, WC–CoCr, WC–NiCr, WC–CoNiCr, and WC–NiCrMo. The wear in such samples was studied, and it was determined that chromium-containing metal binders are characterized by higher wear resistance compared to other composites. The possibility of using SPS to obtain WC–Co composite materials was presented in [41]—two series of composites, different in grain size and cobalt content. In particular, phase analysis showed the occurrence of the WC, Co, and $Co_3W_9C_4$ phases. The lowest

friction coefficient was found in samples sintered using ultrafine powder with an average initial particle size of 400 nm.

To minimize WC grain growth and avoid WC–WC non-metallurgical contacts in WC–Co hard metals, conventional solid-state hot pressing was modified [42] into STSSHP (Short-Time Semi-Solid Hot Pressing) for WC–Co powders consolidation. STSSHP can produce fully dense WC–Co hard metals free of WC–WC non-metallurgical contacts at semi-solid temperatures lower than the ideal liquid-phase sintering temperatures within several to several ten seconds, thus minimizing WC grain growth. The WC–8wt.%Co composition was processed at 1340°C (the WC–Co eutectic temperature) for only ~15 s to achieve a relative density of 99.92%. Only slight WC grain growth occurred. The material exhibited smaller WC grains and thus higher hardness, fracture toughness, and bend strength than those in its liquid-phase sintered counterparts. The method for producing WC–10wt.%Co hard alloy with 99.6% of the theoretical density and Vickers hardness of ~1400 $HV_{0.5}$ was described in [43]. The high-speed powder mixture SPS-consolidation provided a high-quality product within the temperature range of 1000–1200°C.

The operational properties of hard alloys are improved not only by the influence of carbide additives but also by optimizing the composition of the cementing metal components. In this sense, the partial or complete replacement of cobalt in the WC–Co alloy remains a relevant task. Complex metal alloys have been proposed not only to replace cobalt but also to improve the high-temperature characteristics of the alloy. Among the recent results, it is worth noting the creation of a cementitious multi-component metal alloy FeNiCoCr [44], in which the chromium content exceeds 8wt.%. The characteristics of the WC–FeNiCoCr composite depend on the grain size of the matrix material, i.e. WC. Compared to WC–Co of the corresponding composition, the hardness value is essentially preserved, and the toughness is reduced by 25%. The influence of iron Fe and carbon C additives on the physical-mechanical properties of WC–13wt.%Co was studied [45]. The samples were obtained by high-temperature annealing without pressing. It is shown that adding 2wt.%Fe and 1wt.%C gives samples an optimal ratio of hardness and impact toughness. The hardness index increases from 980 to 1070 HV and the bending strength by 9.4%.

It is known that the tool cutting edge is made of tungsten carbide WC, and if it contains boron nitride BN introduced by LD (Laser Doping), it has a very high cutting resource. Considering this circumstance, LD was carried out [46] on the base material of such cutting tools – tungsten carbide–cobalt WC–Co alloy. EBSD (Electron BackScatter Diffraction) and XRD (X-Ray Diffraction) show that changes in the crystal structure are observed only in the 50 nm surface layer. Such LD improved the strength of the material by 11.7% so that the structure of WC was practically preserved. A new method [47] of the WC–8Co hard alloy sintering consists of a repressed, porous billet moving in an induction heating zone. The presence of a liquid phase prevents the growth of tungsten carbide grains. Their size of tungsten at sintering temperature in the range of 1240–1280°C and travel speed of 3 mm/min decreases from 3.9 to 1.9 μm. The structure refinement causes an increase in the hardness from 417 to 664 HV_1.

1.1.2 WC–TiC System

The PCAS was utilized [48] to consolidate ultrafine grain WC–(0–50)at.%TiC cemented carbides. The composition WC–50at.%TiC with a relative density of up to 99% and average grain sizes of about 200 nm was produced within 5 min with the application of 60 MPa pressure. The sintered

composition WC–20at.%TiC had fracture toughness and hardness of 7.5 MPa·$m^{1/2}$ and 2240 kgf/mm^2, respectively. Later, the microstructure and mechanical properties of WC–(0–50)at.%TiC cemented carbides were investigated [49] for samples fabricated by HFIHS (High-Frequency Induction Heating Sintering). Nearly fully dense (with a relative density of up to 98.5%) binderless WC–TiC complex composites were obtained from WC and TiC ultrafine powders with simultaneous application of 60 MPa pressure and induced current for 2 min without significant change in grains average size (about 200 nm).

The WC–TiC composite with different TiC contents in 1–15wt.% was prepared [50] by arc plasma melting in argon. The composite consisted of related carbide, sub-carbide, and mixed carbide phases WC, W_2C, TiC, $TiC_{0.981}$/TiC_{1-x}, and $TiWC_2$/(Ti,W)C, as well as minor/trace phases such as graphitic C, W, and TiO_2. The composite exhibits high hardness and its maximum value of 3650 VHN is observed for the WC–15wt.%TiC sample. Improved hardness was attributed to the presence of additional phases. Open pores' total volume was 0.0002–0.0097 cm^3/g, which, combined with the absence of meso- and macropores, allows us to call this composite a “zero-porosity” material. Young’s modulus also shows significantly high values in the 540–703 GPa range. Simultaneous improvement in the WC–TiC composite hardness and Young’s modulus may be attributed to the growth of new mixed carbide phases of W and Ti and porosity free nature of the material.

1.1.3 WC–TiC–Co System

The growth behavior of two different types of grains, faceted and rounded, in the same liquid matrix was studied [51] in the 70wt.%(75wt.%WC–25wt.%TiC)–30wt.%Co system. Powder samples were sintered above the eutectic temperature under carbon-saturated conditions. (Ti,W)C grains with a rounded shape and WC grains with a faceted shape coexisted in the same Co-based liquid. With increasing sintering time, the average size of (Ti,W)C grains increased continuously, and huge WC grains appeared. The growth of the faceted WC grains resulted in a bimodal grain size distribution. Thus, the growth behavior of one type of grain is not affected by the other kind of grain in the same matrix and is governed only by whether the grain shape is faceted or rounded. Microstructure and mechanical properties of WC–TiC–10wt.%Co cemented carbides fabricated by sintering with HIP were investigated [52]. The WC/TiC grain size ratio was controlled by changing the average size of WC powders, ranging from 0.5 to 4 μm, keeping the average size of TiC powder as 1 μm. At a WC/TiC grain size ratio of 0.5, the TiC/(Ti,W)C core–rim phases were distributed in the WC/Co matrix. While, at WC/TiC grain size ratio above 0.8, these phases were surrounded by the Co binder phase. The hardness of WC–TiC–10wt.%Co cemented carbide increased with decreasing the WC/TiC grain size ratio from 4 to 0.8. However, the hardness at the WC/TiC grain size ratio 0.5 shows much higher values than theoretically expected. Transverse rupture strength of WC–20wt.%TiC–10wt.%Co cemented carbide increases with decreasing the WC/TiC grain size ratio.

WC–TiC–Co system alloys of various compositions are widely used in practice. Such compositions are characterized by high hardness, high-temperature chemical stability, and high wear resistance. Then, they are used to make cutting tools and wear and corrosion-resistant coatings. In recent years, it has been established that obtaining WC–TiC–Co systems in an ultradispersed state and maintaining such a state after compaction significantly improves the physical-mechanical and operational characteristics of the material. WC–TiC–Co systems can be obtained in a nanocrystalline state by sputtering liquid charge and chemical and mechanical methods. The ratio of the constituent

components in a particular system determines their physical-mechanical and operational characteristics. Suppose the composition of the alloy is fixed. In that case, the crucial factors that lead to the improvement of the material mechanical characteristics are the size of the particles, the degree of homogeneity of the structure, and the purity of the initial powder. Thus, it is recommended that the sizes of the carbides, WC and TiC, which make up the WC–TiC–Co system, should be as small as possible – ultradispersed, and their mixture – homogeneous. The sputtering method can be considered promising for obtaining high-purity nanopowders for industrial purposes. However, the application of this method is hindered by the problem identified in the preparation process of the WC–TiC–Co nanostructured system related to the titanium dioxide TiO_2 reduction. A mechanical-chemical method was successfully used to obtain an ultradispersed WC–TiC–Co composite. In particular, its powder with 200 nm particle size was obtained this way [53].

Instrumental metal-ceramic materials of composition titanium diboride–tungsten carbide TiB_2–WC were obtained [54] by VHP (Vacuum Hot Pressing) technique using cobalt Co, nickel Ni, and nickel–molybdenum alloy NiMo as synterability promoting additives. These TiB_2–WC metal-ceramics' microstructure consists of fine tungsten carbide WC and relatively large and uniform grains of titanium diboride TiB_2. Ni_3B_4 brittle phase inclusions and tiny pores were found in the TiB_2–WC–Ni metal-ceramic composite. Many pores and inclusions of brittle phases such as W_2CoB_2 and Co_2B appear in TiB_2–WC–Co metal-ceramics. Cobalt Co liquid phase is mainly spent in reactions forming pores and large grains of TiB_2. The presence of pores, inclusions of brittle phases and large grains in TiB_2 is detrimental to solving the task of improving the mechanical properties of these composites. In this regard, it is worth noting that the sintering-stimulating additive NiMo significantly affects the density and mechanical properties of TiB_2–WC metal-ceramics. The formation of $MoNi_4$ intermetallic compounds is an inhibitor of NiMo liquid phase consumption. On the other hand, the liquid NiMo phase not only inhibits the formation of pores and large TiB_2 grains but also increases the energy of intergranular interfaces of WC and TiB_2. This material is fine-grained, and the average relative density of TiB_2–WC–NiMo metal ceramics is 99.1%. This composite's bending strength, impact toughness and Vickers hardness were 1307 MPa, 8.19 $MPa \cdot m^{1/2}$, and 22.71 GPa, respectively.

In the paper [55], the WC–5wt.%TiC–10wt.%Co powder was mixed by WC – 2.96, (Ti,W)C –2.52, and Co – 2.38 μm and prepared by high-energy ball milling. After 60 h, the powder began to reunite more and more. The average grain size of the powder was 50 nm after 144 h. After 1300–1400°C vacuum sintering the hardness of the sample was 94.8–95.4 HRA, 4.2–5.2 HRA higher than for traditional cemented carbides with the same composition. After 1400°C vacuum sintering the compressive flexural strengths of cemented carbides were 2060 and 1200 MPa, respectively, slightly less than for traditional cemented carbides. The WC–5wt.%TiC–10wt.%Co cemented carbide inserts were prepared and used [56] as the cutting tool for HT250 gray cast iron. The WC–10wt.%Co cemented carbides with the same sintering technology and grain size were prepared for comparison. Adhesive and built-up edges were the predominant tool wear for WC–5wt.%TiC–10wt.%Co cemented carbide inserts. However, attrition was the primary wear mechanism observed in WC–10wt.%Co cutting tools. In work [57], the effect of TiC on WC–Co was studied when it replaced WC by 5–20wt.%. This composite was consolidated by HIP at 1350°C and a 50–150 MPa pressure. When replacing TiC with 5wt.%, the required pressure was 50 MPa, and in the case of 20wt.% – 150 MPa. Substitution of WC with TiC led to an increase in hardness. It increased from 1050 to 1330 HV when replaced by 5wt.%, and up to 1600 HV at 20wt.%. Such a high increase should be due to the addition

of TiC and the reduction of porosity during high-pressure compaction. Young's modulus, on the contrary, decreases with the addition of TiC. If the Young's modulus of WC–Co was equal to 570 MPa, it became 420–490 MPa with the addition of TiC. The impact toughness and density of the composite also decrease slightly with the addition of TiC.

The work [58] discusses the heat treatment processes in two-carbide (WC and TiC) alloys and the effect of laser-impulse treatment on their structure and operational characteristics. It has been established that the microcracks in the surface layers of T15K6 alloy increase by 150–200 units due to laser-pulse impact. Such strengthening is associated with structural and phase transformations caused by electrical-physical effects: a new phase of W_2C is formed in the surface layers, and the binding cobalt phase is saturated with tungsten and titanium carbides. In addition, laser heat treatment increases the operational characteristics of T15K6 by 2–3 times. The work [59] investigated the microstructure and mechanical and tribological properties of tungsten carbide–titanium diboride WC–TiB_2 composite samples sliding on stainless steel (grade 201) surface. As the content of titanium diboride TiB_2 increases from 10 to 30wt.%, the relative density of the material increases, and its mechanical properties improve while the number of microstructure defects decreases. The friction coefficient decreases not only with an increase in the sliding speed but also with an increase in the load. The formation and rupture of composite coatings significantly affect the contact surface, leading to adhesive and abrasive wear mechanisms. The wear rate of WC–TiB_2 composites increases with increasing average load and sliding speed. Finally, the WC–30wt.%TiB_2 composite showed better tribological properties than the WC–20wt.%TiB_2 and WC–10wt.%TiB_2 ones.

Cemented carbide materials were prepared [60] by mixing powders with alcohol, prilling, molding to shape and atmosphere sintering using WC and TiC as the complex phase and Co as the bonding phase. The addition of TiC inhibited the solid solution of tungsten in cobalt and improved the cemented carbides' cobalt content. During the sintering process, WC and TiC react to produce a solid solution of (Ti,W)C with higher hardness. However, with the increasing amount of the TiC, the cobalt and the hardness of the cemented carbides increase while the bending strength decreases. In the process of crack propagation, (Ti,W)C solid solution can deflect the crack orientation, prolong the path of crack propagation, and play a pinning action on the crack, which can toughen the cemented carbides—the addition of various amounts of $TiC_{0.9}$ phase in the range from 5 to 20wt.% substituting WC phase was applied [61] in WC–Co hard metals with 9.5wt.% bonding cobalt phase. The hard metals were consolidated using the HIP method at a temperature of 1300°C and pressure of 1500 atm. The fracture toughness changed from 12 to 9 MPa·$m^{1/2}$. The amount of the $TiC_{0.9}$ phase affected the mechanical and physical properties, changing Vickers hardness from 12.5 to 14.0 GPa, Young's modulus from 550 to 460 GPa, density from 13.1 to 9.6 g/cm^3, friction coefficient from 0.24 to 0.45, and fracture toughness from 16.8 to 11.0 MPa·$m^{1/2}$.

One of the most applied approaches to improve the WC–Co cemented carbide performances is the addition of transition metal carbides such as TiC, which prevents diffusion wear thanks to the gamma-phase (Ti,W)C formed during sintering. In order to understand the thermal metallurgical reactions that occurred between WC–Co cemented carbide and TiC transition carbide and its effect on the microstructural and mechanical properties, a cemented carbide composition was elaborated [62] by conventional powder metallurgy. Its microstructure was a mixture of angular WC grains and (Ti,W)C rounded grains embedded in the Co-rich binder. These three phases were presented with small amount of free carbon revealed by solution–reprecipitation phenomena caused by liquid

phase sintering. The study [63] investigated the effect of near-nano-TiC additions on microstructural development and densification, increasing hardness and wear resistance. Standard WC–13Co powder mixture was modified with 2wt.% TiC powders with an average of 350–400 nm grain size.

The WC–Co/(Ti,W)C graded cemented carbide was prepared [64] by SPS. The substrate was WC–8wt.%Co, and the hard layer was (Ti,W)C solid solution. The hard layer was mainly formed by dissolving WC in the Co-phase and then by solid-solution reaction with TiC. As the sintering temperature increased, the migration rate of WC increased. When the holding time was 5 min, the thickness and the W content of the (Ti,W)C solid solution hard layer increased with the increasing sintering temperature. The thickness of the (Ti,W)C solid solution can reach 51 μm at the sintering temperature of 1700°C for the holding time of 5 min. The hardness of the hard layer surface increases first and then decreases with the increasing sintering temperature. The Vickers hardness $HV_{0.2}$ is the highest at 1600°C, which can reach 21.53 GPa. As the holding time increases, the thickness of the solid-solution hard layer increases, but the growth rate decreases. As the thickness increases, the difference in the W element concentration between the solid solutions of the same pitch decreases along the layer depth direction, and W element concentration in the entire hard layer increases. The (Ti,W)C hard layer has superior oxidation resistance relative to the WC–Co substrate. The study [65] synthesized functionally graded WC–TiC–Co cemented carbides with a unique bilayer microstructure by high-pressure nitriding sintering. A fcc (face-centered-cubic) phase-riched surface layer and an intermediate layer (cobalt-rich and coarse-WC grain) are formed. With the increasing of initial WC particle size, the carbide grain size of the surface layer, the intermediate layer, and the inner region increase after sintering. The intermediate layer shows significantly coarser WC grains than the inner region. The thickness of the bilayer increases with the increment of initial WC particle size, which indicates that ultrafine WC grains constrain the gradient microstructure formation.

The paper [66] presented a method for producing a hard alloy WC–5wt.%TiC–10wt.%Co with a density equal to 100% of the theoretical value, a hardness of 1484 HV, and a bending strength limit of 1924 MPa. The high quality of the product was ensured by a method based on the mechanochemical synthesis of WC and TiC powders using available precursors and the implementation of high-speed SPS consolidation of the obtained powder while achieving a high degree of packaging with a minimum grain growth at 1200°C and processing time no more than 13 min. The WC–(Ti,W)C–Co hard metal was fabricated [67] using carbon black, WC, Co, WO_3, and TiO_2 as raw materials through an energy- and cost-efficient method that the process of carbothermal reduction of oxides and the liquid phase sintering of hard metal were combined in one heating cycle. The in-situ carbothermal reactions and outgassing processes had finished below 1200°C. Microstructures of hard metals consist of WC grains, (Ti,W)C solid solution, and Co binder phase. The mean size of WC and (Ti,W)C grains were smaller than those of hard metal prepared with TiC powders. A coherent relationship between Co and (Ti,W)C grain was noticed, and a cohesive relationship between two (Ti,W)C grains was observed. Hard metals prepared through this method showed good mechanical properties with hardness of 90.7 HRA, transverse rupture strength of 3007 MPa, and fracture toughness of 13.1 $MPa \cdot m^{1/2}$.

Cemented carbide of composition 91wt.%WC–3wt%TiC–6wt.%Co was SPS-ed [68] at temperatures of 1200, 1300, and 1400°C and the effect of sintering temperature on this type of composite microstructure and properties (total and apparent densities, hardness, fracture surface, etc.) were investigated. The evident density increased with increasing sintering temperature from

1200 to 1300°C from 13.98 to 14.23 g/cm^3, respectively. Nevertheless, the density of the sample sintered at 1400°C was reduced to 14.20 g/cm^3. Initially, increases in fluidity and capillary pressure of the cobalt phase cause an increase in density. At higher temperatures, cobalt evaporates and the density slightly decreases. The number of TiC-core–(Ti,W)C-shell structures increased with the increase in sintering temperature. As a result, the hardness also increased. Its value of 1746 kgf/mm^2 obtained for the sample sintered at 1200°C increased with increasing sintering temperature from 1300 to 1400°C from 2094 to 2280 kgf/mm^2, respectively. At the optimum sintering temperature, TiC inhibited the growth of tungsten carbide in the WC grains. PMF (Pulsed Magnetic Field) with different intensities was used [69] to treat the WC–TiC–Co inserts to improve their properties, microstructure and cutting. About 17% decrease in the cutting force is achieved at 57 and 20% reductions for the flank and notch wears, respectively. Vickers hardness increases slightly at the optimum process parameter. At the same time, PMF significantly improves the insert microstructure by enhancing the martensitic transformation of the α-Co phase into ε-Co and dislocations multiplication. The PMF presence reduces the texture anisotropy, which leads to the formation of a uniformly refined microstructure.

1.2 B_4C–W Composites

B–C–W ternary system composites can be obtained by modifying the previously developed [70-75] liquid charge method for boron carbide B_4C matrix multicomponent ceramics containing tungsten W compounds.

Boron carbide–tungsten B_4C–W composites with 5, 10, 15, and 20vol.% of metallic tungsten were obtained [76] by SPS technique by heating in vacuum from room temperature to 1500–1600°C at a rate of 100°C/min and under the influence of a pressure of 40 MPa directed along an axis for 4 min. Commercial powders of boron carbide B_4C and tungsten W with average particles sizes of 0.7 and 60 μm and purity of 99.5 and 99.8%, respectively, were used. The powder mixture was prepared by grinding the mentioned components in a tungsten carbide WC ball mill in an ethanol medium for 24 h. The tungsten boride W_2B_5 (boranylidine) phase was formed due to a reaction between boron carbide B_4C and tungsten W particles. As more tungsten is added, a graphite phase also appears. An increase in the amount of graphitic carbon C worsens the material's mechanical properties, while the addition of metallic tungsten improves the sinerability of the B_4C matrix and densifies it. The ability of the boron carbide–tungsten B_4C–W composite samples with near-theoretical density to attenuate gamma- and neutron-fluxes was also investigated. It was concluded that increasing the proportion of W in the B_4C–W system leads to a more substantial attenuation of the gamma-ray flux. It also decreases the protection from thermal neutrons compared to monolithic B_4C.

For borocarbide ceramics, pressureless sintering is a method of industrial value. However, they cannot be sintered to high densities without special additives that promote densification. Such sintering additives and metallic tungsten W, together with the corresponding methods of sintering, such as SPS, PECS, and PPC, were described in the review [77]. Sintered WC–WB–W_2B composites were prepared [78] from tungsten borocarbide-containing B_4C–W–WC powders by VHP using a reactive energization technique that initiated a solid-state reaction between B_4C and W. In the case of a molar fraction of WC equal to 0.769 in the initial powder, WB and WC phases are formed as a result of the reaction $B_4C + 5W + xWC = WB + (1 + x)WC$, and WB, W_2B and WC phases are formed if its molar fraction exceeds 0.854.

Due to the high value of the (epi)thermal neutrons capture cross-section by boron ^{10}B isotopes, boron and its compounds and composites are widely used as materials intensively interacting with neutron radiation. They exhibit additional properties that improve their functional characteristics in finely dispersed form. In particular, information is available [79, 80] about obtaining such essential boron-containing finely dispersed B_4C–W composites, which are useful in neutron shielding. Initially, tungsten oxide WO_3 is coated on the surface of boron carbide B_4C using the so-called centrifugation method, and the obtained layer is then sintered at a temperature of 600–800°C in a hydrogen atmosphere to reduce it to α-W. The metallic tungsten layer is often weakly bonded to the B_4C surface. The SPS method was the most effective for obtaining such composites in sandwich structures at a temperature of 1300–2000°C. For this purpose, the previously developed method was modified by which tungsten-containing B_4C-matrix multicomponent ceramics were obtained. An ultradispersed boron carbide powder consolidated by SPS at 1500–2000°C is used as the base layer obtained by the wet method from boric acid–organic compound–water, amorphous boron–carbohydrates–water, and other similar systems. When such sandwich structures are heated at temperature >1300°C, the formation of tungsten pentaboride W_2B_5 begins, and at >1600°C a new sandwich composite B_4C–W_2B_5 is formed. Using the SPS method, multicomponent layered structures can be made from two-component sandwiches: B_4C–W–B_4C, W–B_4C–W, B_4C–W–B_4C–W, W–B_4C–W–B_4C, etc. The same SPS method was used to obtain monolithic B_4C–W samples from boron carbide and tungsten powders. For this purpose, metallic tungsten powder was placed in a graphite mold lined with graphite foil and compacted. Boron carbide powder was then coated with layer of powdered tungsten. The surface was leveled and covered again with graphite foil. In this approach, the powder is consolidated by rapid heating and some pressure to form a composite in a sandwich form. As shown by the SEM (Scanning Electron Microscopy) and EDX (Energy Dispersive (micro)X-ray) studies of the fractured surface of the structure on the contact surface of the consolidated B_4C and W phases, the diffusion of B and W atoms in opposite directions and the formation of the intermediate W_2B_5 phase takes place. In addition, the thickness of the layers can vary widely. After removing the tungsten and boride layers from the sample sintered at 1600°C, boron carbide's relative density was 87–92% of the theoretical value. XRD analysis of the cleaned surface unambiguously confirmed the presence of metallic tungsten and its removal from the sandwich surface. A method of obtaining similar composites using metal tungsten plates was also developed. It was found that by heating and pressing boron carbide powder and metallic tungsten foil, intermediate phase W_2B_5 is formed, which provides strong adhesion between these two phases.

From the conducted modeling [81-83], it follows that boron carbide–tungsten B_4C–W thin-layer sandwich structures are effective neutron radiation shielding composites, in which atoms with small and large Z (Z is the atomic number), i.e., boron B and tungsten W provide effective absorption, respectively, for (epi)thermal neutrons and secondary gamma-quanta, which emission accompanies the capture of neutrons by the nuclei of the boron ^{10}B isotopes.

The effect of interfacial roughness on the reflectivity of boron carbide–tungsten B_4C–W multilayer composite varying with the number of bilayers N was specifically investigated [84] for such systems by design, with the period of 2.5 nm thickness. A realistic structural model was used to calculate the reflectivity changes for N = 50, 100, 150, and 200. These multilayer systems were produced in a DC (Direct Current) magnetron sputtering facility. Their reflection and scattering intensities were measured by the XRD method. The results indicate that the reflectance is a function

of the number of bilayers in the structure, and the interfacial roughness increases slightly from a given layer to the next layer as the multilayer structure grows.

An experimental study of the preparation of two tungsten borides, namely WB and W_2B_5, by SHS [85] was carried out, during which borothermal reduction of tungsten oxide WO_3 took place by the interaction of tungsten W with boron B. The reactant compact's initial stoichiometry essentially affects the final product's combustion course and phase composition. The addition of metallic tungsten and boron decreased the overall exothermicity of the reaction, leading to a decrease in both the combustion temperature and the reaction front movement velocity. Composites obtained in situ tungsten pentaboride W_2B_5 and graphite C containing boron carbide B_4C were synthesized [86] by an annealing technique. Initial powders of B_4C containing 5vol.%W were formed into bulk composites. The annealing process was carried out at temperatures of 1500, 1550, and 1600°C in vacuum. The effect of tungsten additions and different annealing temperatures on material densification, hardness, impact toughness, and microstructural properties were investigated.

1.3 Recycling of W-containing Waste

Tungsten-containing alloys are widely used in modern technology, and the demand for this material is increasing daily. The scarcity of tungsten led to its removal from tool scrap and reused to make complex instruments. Methods for extracting tungsten from tungsten-containing scrap have been developed for decades. Some methods implemented in practice have particular strengths and weaknesses. In general, when selecting ways to process such waste, it is crucial to consider productivity (yield), simplicity of the technological process, environmental friendliness of the method used, and, as far as possible, low energy costs. The ways of processing wastes of tungsten-containing hard materials are given in the book [87].

Here are the main methods to recycle such waste and produce tungsten-containing hard alloys.

(1) Crude dispersion of sintered waste with different crushers and then grinding the obtained mixtures into finely dispersed fractions. The method is characterized by low performance, which causes the grinder to wear out quickly. Another version of the same process is to extract cobalt from waste by heating it to 2300–2500°C. After the cobalt is removed from the material, it disperses. The disadvantage of this version is that cobalt is completely lost from the system when used.

(2) The complete decomposition of waste by chemical-metallurgical method occurs in a special furnace in strong oxidizers – alkaline nitrates and nitrites. Then, it is poured, crushed, and leached with hot water. These hydrometallurgical processes are somewhat analogous to the production of polyvinyl chloride: $WC + 2NaNO_3 \rightarrow Na_2WO_4 + CO_2 + N_2$ and $2Co + 2NaNO_3 \rightarrow Co_2O_3 + 2NO + Na_2O$. This method is used in some industries but has disadvantages, such as multistage routes and releasing toxic gases in the process.

(3) Selective separation of cobalt from the solution is done by heating it and treating it with acid or alkali. This process is relatively slow and unprofitable.

(4) The method of chlorination is multistep. Its main principle is to obtain tungsten and cobalt chlorides and their mutual separation: $2WC + 6Cl_2 + O_2 \rightarrow 2WCl_6 + 2CO$ and $Co + Cl_2 \rightarrow CoCl_2$ (800–850°C). Two high-purity compounds are obtained and separated in distillation columns. Then, they are converted into oxides and reduced. The feature of this method is the chlorination of the waste at a temperature of 900–1100°C in the presence of carbon dioxide

CO_2, which forms a surface layer of graphite. Cobalt chloride condenses at 900°C on one condenser, and tungsten, titanium, and tantalum chlorides condense on another. Then they are purified. The disadvantage of this method is the need to work with environmentally dangerous material – chlorine.

(5) The process is slow in the method that involves heating the waste to 1100°C, oxidizing it in air, and recovering the product WO_3. The formed cobalt tungsten reduces the possibility of completely removing tungsten from the solution.

(6) A method that involves oxidizing the waste and then chlorinating it means trapping the tungsten chloride and leaving the cobalt dioxide in the chlorinator. The disadvantage of this method is that it releases dangerous gases during the technological process.

(7) In the electrochemical or electrolytic method, ammonia and alkaline solutions and salts are processed. During the electrolyte's selective electrochemical dissolution of complex alloy components, tungsten carbide WC does not have time to oxidize to tungstic acid and precipitates into insoluble anode sludge. Therefore, the disadvantage of this method is the need for subsequent annealing of tungsten carbide to obtain its oxide WO_3.

(8) Methods of sawdust processing are essentially hydro- and pyrometallurgical. For example, according to one technology, dusty tungsten-containing waste generated during tool sharpening, after sifting, is subjected to leaching with sulfuric acid and decontamination of tungsten concentrate using pyrolusite. The solution is neutralized with soda and pumped into a sludge storage tank. The resulting pulp settles, and the top layer is sent to the filter press. Tungsten concentrate in the form of sediment from the filter press is blown with compressed air. This product can be used in the smelting of ferrotungsten.

(9) The method of processing with regenerators of the mixture includes fine-grained grinding with a high-energy air stream, quenching of hard alloys in ice water at 1300–1400°C (cracks are formed in the alloy in the case of a massive sample), and then crushing the forged mass.

(10) Tungsten powder can be obtained from waste by the following scheme: dissolution with sodium hydroxide, precipitation in hydrochloric acid, precipitation and purification of ammonium paratungstate with ammonia, and reduction to tungsten with hydrogen.

(11) Thermal regeneration means an oxidation–reduction–carbonization process.

(12) Cobalt extraction with zinc and then vacuum distillation is the so-called zinc method widely used today.

The regeneration process of hard alloys is also processed under the influence of shock waves. This highly efficient production technology allows, without thermochemical and metallurgical processes, through the direct regeneration of secondary raw materials, obtaining the powders of hard alloys useful to create tools. The technology fundamentally differs from the existing ones regarding high technical and economic indicators, high performance, low energy consumption, and environmental friendliness [88]. The recovery of the tungsten-containing mixture is carried out under high-pressure gradient conditions, and delivery velocities in cylindrical reaction ampoules are subjected to the impact caused by the detonation of an axially symmetric explosive charge.

In this paper, ultradispersed metal-ceramic powders of different concentrations are obtained by chemical synthesis and mechanical dispersion in the attritor. To improve the operational characteristics of tungsten carbide-based hard materials, they are alloyed/modified with ceramic phases, namely, ceramic quasieutectic alloy B_4C–30wt.%TiB_2 of boron carbide B_4C and titanium diboride TiB_2. The obtained metal-ceramic powders are compacted using SPS and HTS (High-

Temperature Sintering) methods. The phase composition of the obtained composites is studied using the XRD method. The PDF-2 (Power Diffraction File-2) and COD (Crystallography Open Database) were used to analyze the diffraction images. Chemical element distribution maps are obtained by EDX spectrometry. Structural features are investigated using optical and electron microscopies. The main physical-mechanical characteristics of the obtained samples, such as hardness, microhardness, and bending strength, are also studied.

2. WC–Co Alloy Modified with B_4C–TiB_2 Composite

2.1 Chemical Synthesis of Ultradisperse WC–Co Alloy Using Different Precursors

Two groups of precursors were selected for obtaining by chemical method the ultradispersed WC–Co alloys using suspension solutions: (1) Ethyl alcohol solution of tungsten chloride $WCl_6 \cdot 6H_2O$, mixture of aqueous solution of cobalt chloride $CoCl_2 \cdot 6H_2O$, and alcohol solution of neurotrophin $C_6H_{12}N_4$; and (2) Aaqueous suspension of ammonium tungstate $(NH_4)_{10}(H_2W_{11}O_{41}) \cdot 4H_2O$, cobalt acetate $Co(CH_3COO)_2 \cdot 4H_2O$, and sucrose $C_{12}H_{22}O_{11}$ (as carbon source).

Figure 1 presents the XRD image of WC–Co obtained with precursors such as tungsten, cobalt chlorides, and urotropin. The method of obtaining nanocrystalline tungsten carbide with these components was developed by the authors of this paper [89]. It is known that in synthesizing tungsten carbide, the presence of such intermediate complex carbides (mainly W_3Co_3C and W_6Co_6C) in the final product is expected, which causes degradation of the physical-mechanical properties of the material. By optimizing the technological parameters, it was possible to obtain the final product without these intermediate carbides. Table 1 shows the component phases of the synthesized composite powders depending on the synthesis temperature and duration.

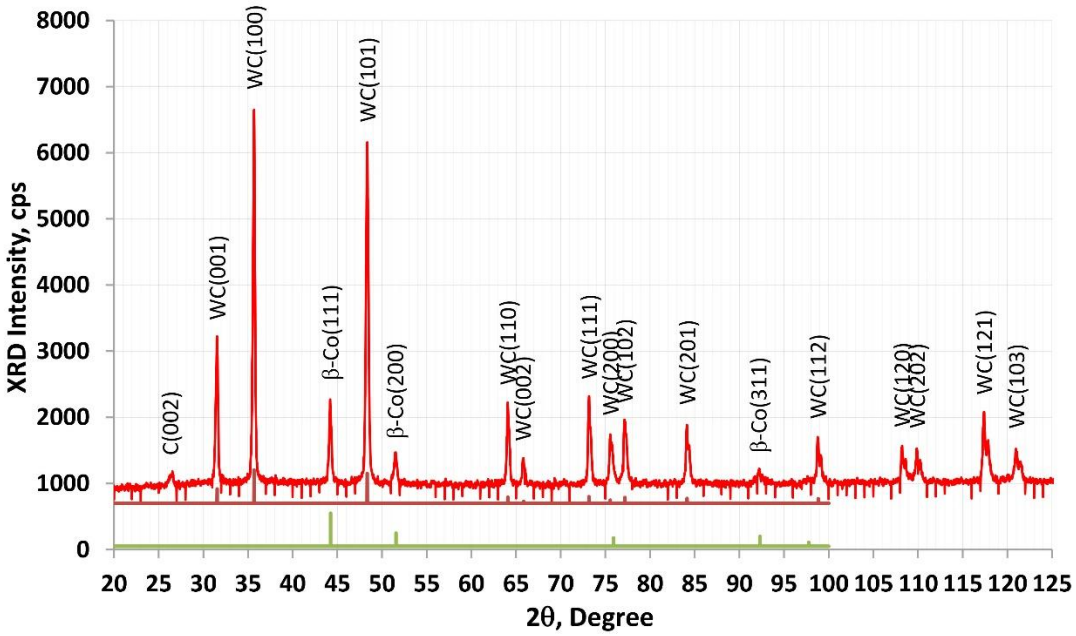

Figure 1 XRD image of WC–Co alloy synthesized at a temperature of 1000°C for 1.5 h using tungsten and cobalt chlorides and urotropin (WC – Leciejewicz and β-Co – pdf 15-806).

Table 1 Dependence of technological parameters on powder samples' phase composition synthesized using tungsten, cobalt chlorides, and urotropin.

#	Synthesis parameters		Phase composition
	Temperature, °C	Duration, h	
1	750	0.5	$WC–W_2C–W_3CCo_3–W_4CCo_2–W_6CCo_6$
2	750	1	$WC–W_2C–Co_3W_3C–W_4CCo_2–W_6CCo_6–Co$
3	750	2	$WC–W_2C–W_3CCo_3–W_6CCo_6–Co$
4	850	0.5	$WC–W_2C–W_3CCo_3–W_6CCo_6–Co$
5	850	1	$WC–W_3CCo_3–W_6CCo_6–Co$
6	850	2	$WC–W_6CCo_6–Co$
7	950	0.5	$WC–W_6CCo_6–Co$
8	950	1	$WC–W_6CCo_6–Co$
9	950	2	WC–Co

Structural features of synthesized composite powders are studied. Figure 2 shows an SEM image of a composite powder synthesized using tungsten, cobalt chlorides, and urotropin. It is an ultradisperse of the powder in agglomerated blocks with a nanoscale particle size of ≤100 nm.

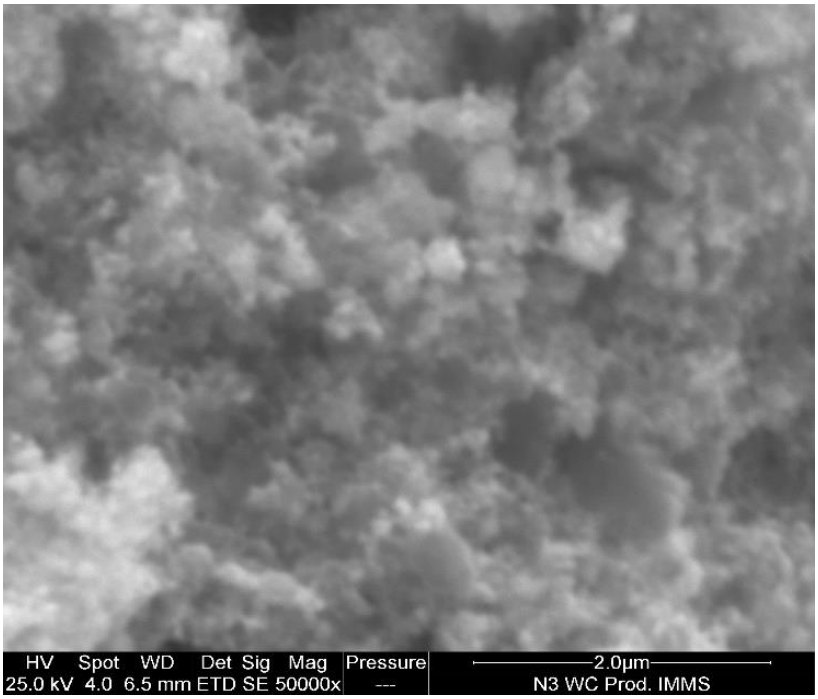

Figure 2 SEM image of powder synthesized using tungsten, cobalt chlorides, and urotropin.

Since the processes involving chlorides are environmentally undesirable, precursors of the second group were also used to obtain nanocrystalline WC–Co. Figure 3 presents the XRD image of WC–8wt.%Co synthesized (750°C and 0.5 h) using ammonium tungstate, cobalt acetate, and sucrose suspension aqueous solution.

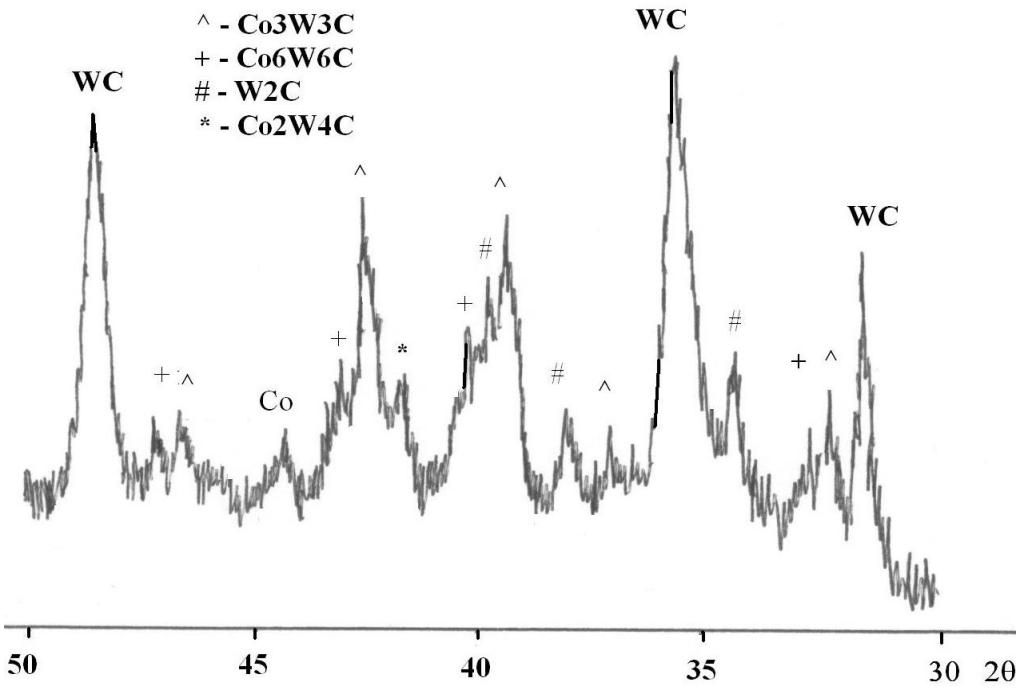

Figure 3 XRD image of WC–8wt.%Co synthesized (750°C and 0.5 h) using an aqueous suspension of ammonium tungstate, cobalt acetate, and sucrose.

One more method of obtaining nanocrystalline tungsten carbide is also proposed. Ammonium paratungstate $(NH_4)_{10}W_{12}O_{41}$, urea $CO(NH_2)_2$, 65% solution of nitric acid HNO_3, and glucose $C_6H_{12}O_6{\cdot}H_2O$ were used as precursors. Such low-temperature synthesis is based on oxidation–reduction reactions. Preparation of liquid charge involves dissolving $(NH_4)_{10}W_{12}O_{41}$, $CO(NH_2)_2$, and $C_6H_{12}O_6{\cdot}H_2O$ components in deionized water and then adding 65% HNO_3. To dehydrate the obtained solution, it was placed in a closed oven heated to 500°C. After the intense release of water vapor and gaseous reaction products, the solution becomes a foamy jelly-like mass, initiating a strongly exothermic autonomous combustion process. As a result, a black-colored combustion product is obtained, which is used as a precursor to obtain WC. Activated carbon in the form of carbon black is added to this intermediate product, and they are mechanically mixed and heat-treated at 800–1100°C in an argon stream.

Figure 4 presents the XRD image of the product treated at 1100°C. Phase composition analysis revealed that the main component phase is the target product WC. However, other tungsten-containing phases, such as W, WO_3, and H_2WO_4 are also observed, indicating a lack of carbon in the reaction system. Studies to determine the reactants' stoichiometric composition and the reaction's thermal regimes are ongoing. According to the diffraction maxima at 2Θ = 35.684 and 48.344°, the sizes of the obtained tungsten carbide crystals were estimated to be 32 and 31 nm, respectively, by Scherer’s method.

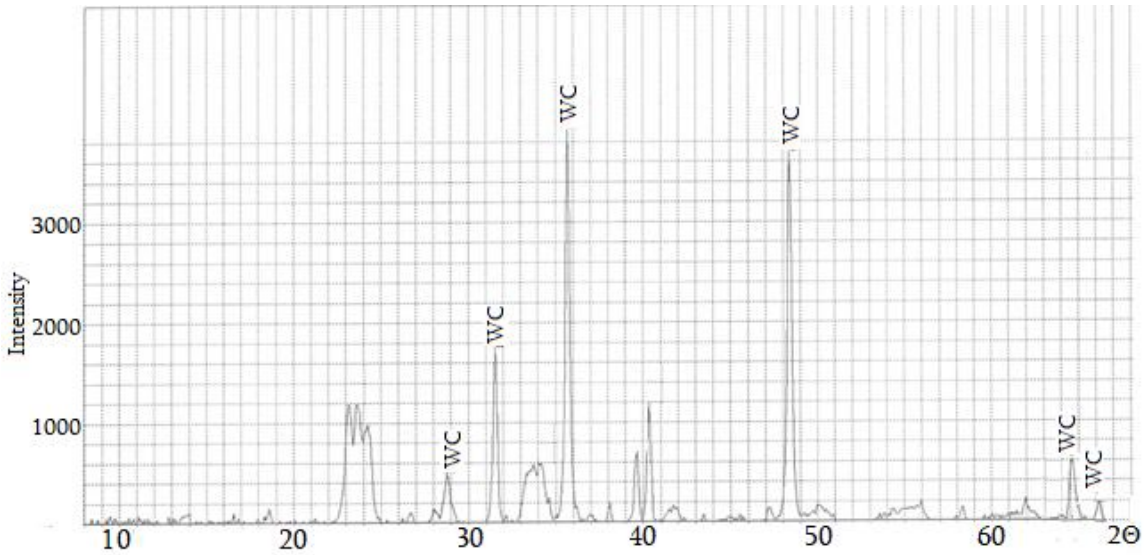

Figure 4 XRD image of tungsten carbide synthesized at a temperature of 1100°C using ammonium paratungstate $(NH_4)_{10}W_{12}O_{41}$, urea $CO(NH_2)_2$, nitric acid HNO_3 65% solution, and glucose $C_6H_{12}O_6 \cdot H_2O$.

2.2 Preparation of Ultradisperse B_4C–TiB_2 Modifier by Chemical Synthesis and Mechanical Dispersion

As is known, boron carbide is characterized by high hardness and low thermal conductivity, which hinders the production of complex-shaped products from it and the material's thermal stability. To increase the field of applications of B_4C, it is necessary to resolve these problems by introducing appropriate additives into the material. From this point of view, the titanium diboride TiB_2 is attractive due to its high thermal conductivity hardness, and forming a pseudobinary alloy with boron carbide (Figure 5).

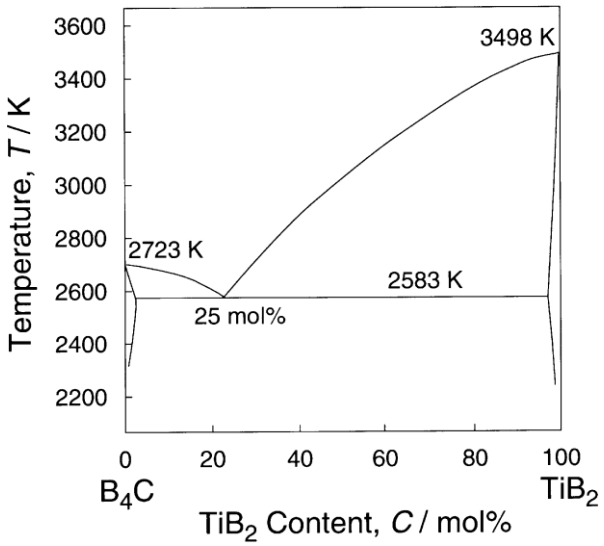

Figure 5 Phase diagram of B_4C–TiB_2 pseudobinary alloy.

The authors of work [90] obtained the B_4C–TiB_2 quasieutectic alloy by electron-beam zone melting. The TiB_2 phase is embedded in the B_4C matrix as a continuous rod, and the growth

directions of the phases form an angle of 22° to each other. The electrical conductivity of the composite, measured in the direction of crystal growth, is increased by 2–3 orders of magnitude compared to monolithic B_4C. Accordingly, its thermal conductivity also increases, and the microstructure of the composite is almost similar to the microstructure of boron carbide. Thanks to the high thermal and electrical conductivity, it is possible to process the sample of this composite using the electric erosion method and give it the desired geometric shape. This alloy, with its unique properties as a modifier of hard alloys, should significantly affect the properties of WC–Co, in particular.

Quasieutectic binary alloy B_4C–TiB_2 in the ultradispersed state was obtained by the authors of this work [91]. The method of securing boron carbide-based nanocrystalline hard material provided simultaneous synthesizing of B_4C and TiB_2 using liquid charge. The charge was a suspension solution consisting of powdered titanium dioxide TiO_2, amorphous boron, glycerin, and water. The suspension was dehydrated by drying at 100–110°C and then by step-wise heat treatment of the obtained mass at temperatures of 600–800 and 1250–1300°C. The quantities of charge components were stoichiometrically calculated based on the condition that obtaining powder composites of boron carbide and titanium diboride in the nanocrystalline state with the appropriate ratio of quasieutectic composition would be possible. The SEM image of the obtained composite presented in Figure 6 shows that the central part of the composite's nano-sized powders consists of crystals of a faceted shape characteristic of boron carbide, at least one dimension of which is ≤100 nm. In Figure 7, the phase analysis results are given in the form of an XRD image.

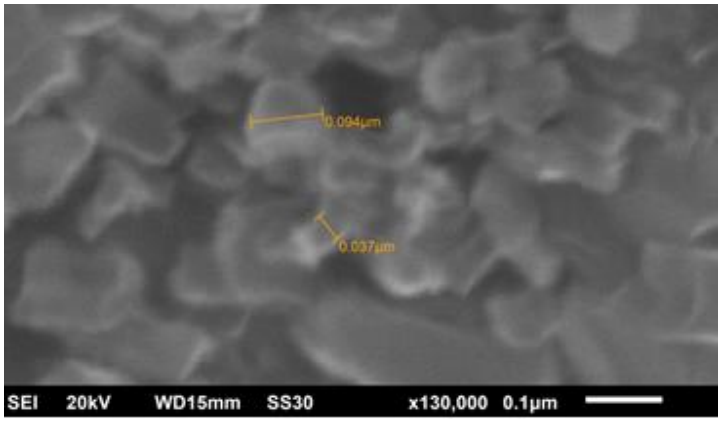

Figure 6 SEM image of powder nanostructured composite obtained on the basis of boron carbide and titanium diboride.

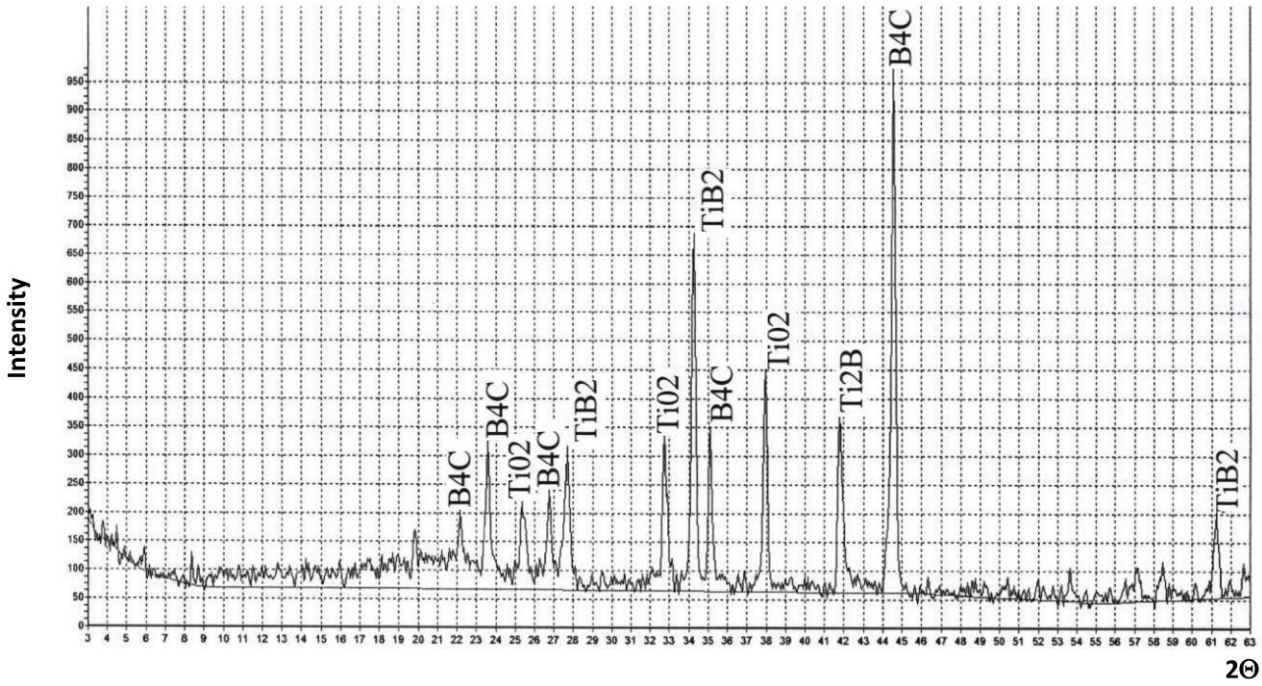

Figure 7 XRD image of powder nanostructured composite obtained on basis of boron carbide and titanium diboride.

We replaced glycerin in a previously developed suspension liquid charge with sucrose, characterized by high solubility in water. The quantities of other components were calculated to obtain wt.% ratio of B_4C:TiB_2 = 70:30 in the two-component ceramic system. The technological parameters remained the same, which we had established in the case of the previously used charge. XRD analysis (Figure 8) shows that the formation of the B_4C–TiB_2 quasibinary system is possible in a single technological process. Figure 9 shows the SEM image for spectral analysis of B_4C–30wt.%TiB_2 quasieutectic alloy powder with spectra markers in four different crystals. The EDX spectrum of one of them (namely, Spectrum 9) is given in Figure 10 in the form of distribution of constituent elements B, C, and Ti, and the spectral analysis results are summarized in Table 2.

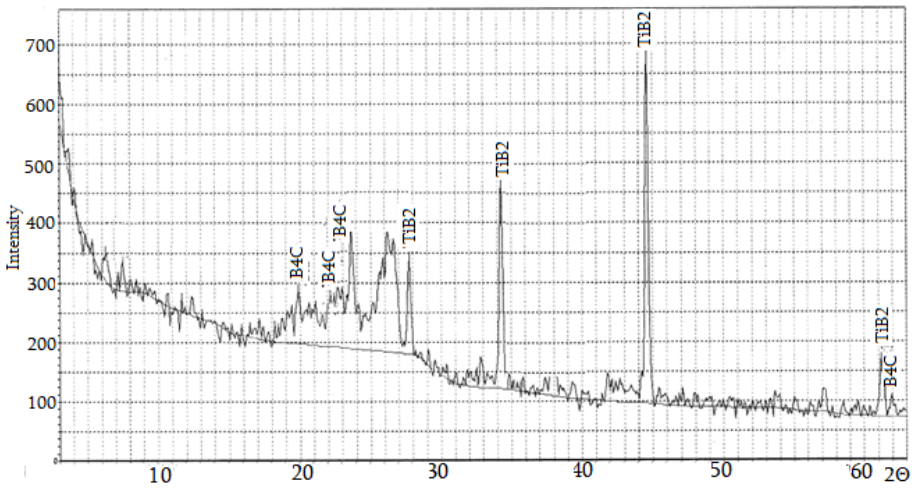

Figure 8 XRD image B_4C–TiB_2 quasibinary system obtained from liquid charge containing titanium dioxide, amorphous boron, sucrose, and water.

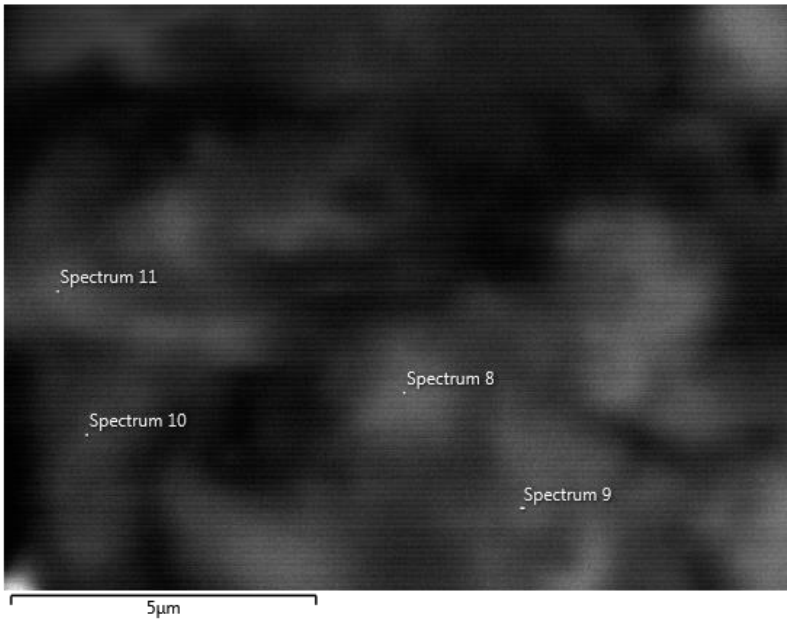

Figure 9 SEM image of B_4C–30wt.%TiB_2 quasieutectic powder obtained from liquid charge containing titanium dioxide, amorphous boron, sucrose, and water.

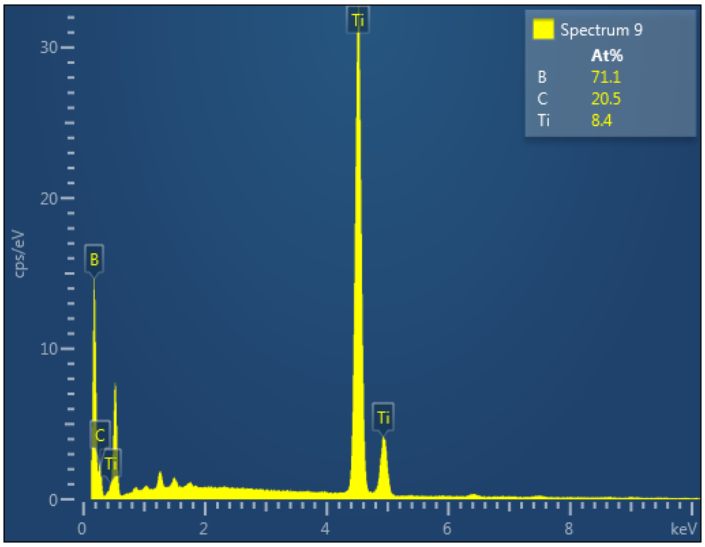

Figure 10 EDX spectrum of chemical elements distribution in B_4C–30wt.%TiB_2 powder quasieutectic.

Table 2 Results of EDX spectral analysis of chemical elements distribution (at.%) in powder B_4C–30wt.%TiB_2 quasieutectic composition.

Chemical element	Spectrum 8	Spectrum 9	Spectrum 10	Spectrum 11
B	65.56	71.12	65.81	66.97
C	27.90	20.50	29.08	29.34
Ti	6.54	8.38	5.11	3.70
Total	100.00	100.00	100.00	100.00
Statistics	**B**	**C**	**Ti**	

Maximum	71.12	29.34	8.37
Minimum	65.56	20.50	3.70
Mean	67.37	26.70	5.93
Mean square deviation	2.58	4.18	2.00

The B_4C–TiB_2 quasibinary system was also obtained by mechanical dispersion. Commercial powders of B_4C and TiB_2 with a purity of not less than 99.5% were used. The initial powder particle size was ≤5 μm. The dispersion process was carried out with planetary minimill Fritsch-6 (Germany) using the wet grinding method. The grinding cup and balls were made of hard WC–Co alloy. The total grinding time was at least 18 h. In this way, a composite powder with a particle size of ≤800 nm was obtained.

Briquettes compacted by pressing with 5 MPa were thermally treated at 2100°C in the high-temperature furnace of the SShV-type in an inert (argon) atmosphere. The obtained monolithic briquettes were crushed in the first stage in a cast iron crusher. In the next stage, when the particle size became less than 0.5 mm, the grinding process continued in the planetary mill, and they were dispersed in the same manner as the initial components. In this case, too, the size of the dispersed grains was ≤800 nm.

2.3 Preparation of WC–Co Alloy Modified with B_4C–TiB_2 Composite

Three methods were selected for obtaining the B_4C–TiB_2-modified WC–Co alloy: (1) Obtaining the target composite by making a suspension liquid charge with the corresponding precursors of the system components; (2) Mixing of separately synthesized ultradisperse B_4C–TiB_2 and WC–Co alloys by chemical method in an attritor-type high-energy mill; and (3) Obtaining a WC–Co–B_4C–TiB_2 metal-ceramic composite of desired components concentration by wet dispersion of B_4C, TiB_2, WC, and Co powders in a high-energy mill. With the first and second methods, it is possible to obtain a composite with an average grain size of ≤0.3 μm, and with the third method ≤0.8 μm. In all three cases, the wt.% ratio of B_4C and TiB_2 components is the same and corresponds to 70:30, while their total amount in the composite varies from 3 to 30wt.%. The Co content varied from 8 to 20 wt.%.

For the formation of the ultradispersed WC–Co–B_4C–TiB_2 system by Method 1, the appropriate precursors of the components were selected, by using which the charge was prepared in the form of paste. The ingredients in this paste are ammonium paratungstate, titanium dioxide, cobalt acetate, sucrose, and amorphous boron. Heat treatment of the resulting paste was performed at temperature of at least 1000°C because WC–Co alloy is formed at this temperature.

It is known that this alloy is often used to obtain tungsten pentaboride W_2B_5. The proposed method allows us to get this phase as an intermediate product. Sucrose-derived pyrolytic carbon reduces tungsten from a mixture of ammonium paratungstate and cobalt compound, which presumably interacts with elemental boron in the charge to synthesize W_2B_5 since the listed charge components were already present in the paste.

The constituent phases of the target material – B_4C, TiB_2, WC, and Co – are formed by simple technology at relatively moderate temperatures: 800–1000°C. However, W_2B_5 tungsten boride begins to form from such a charge at 1000°C (Figure 11). 1000°C is the lowest temperature at which W_2B_5 was obtained. The experiment showed that the initial mixture transforms when gradually heated to 1000°C. According to work [92], pyrolysis of sucrose in a nitrogen atmosphere at 500°C

produces an intermediate product with pyrolytic carbon content of 21–28%. This amount depends on the mixture's type and amounts of other compounds. According to experimental data, the yield of carbon from the WO_3–TiO_2–$C_{12}H_{22}O_{11}$ mixture at 600°C is 19–22%. About 20 g of pyrolyzed carbon is obtained from 100 g of sucrose. By XRD phase analysis, it can be concluded that WO_3 and $WO_{2.90}$ phases are formed by heat treatment of $(NH_4)_{10}(H_2W_{11}O_{41})\cdot 4H_2O$ at 600°C in argon (Figure 12a).

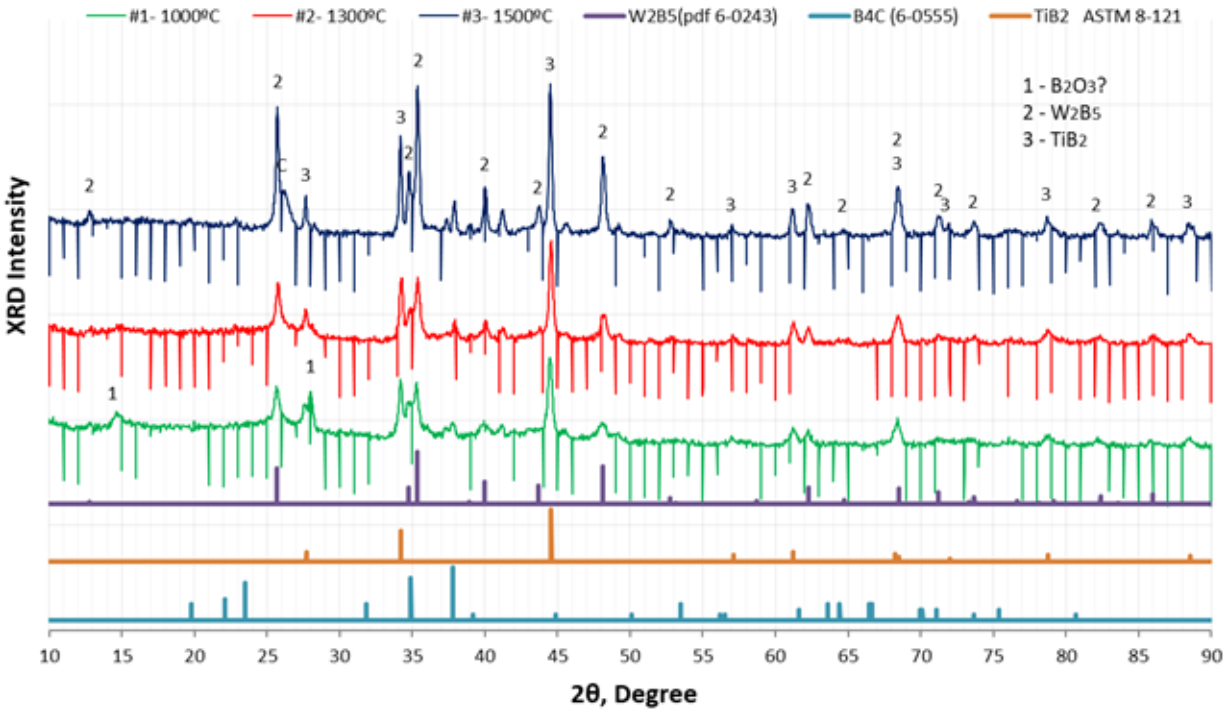

Figure 11 XRD images of the reaction mixture of amorphous boron, titanium dioxide, ammonium paratungstate, cobalt acetate, and sucrose at temperatures between 1000–1500°C.

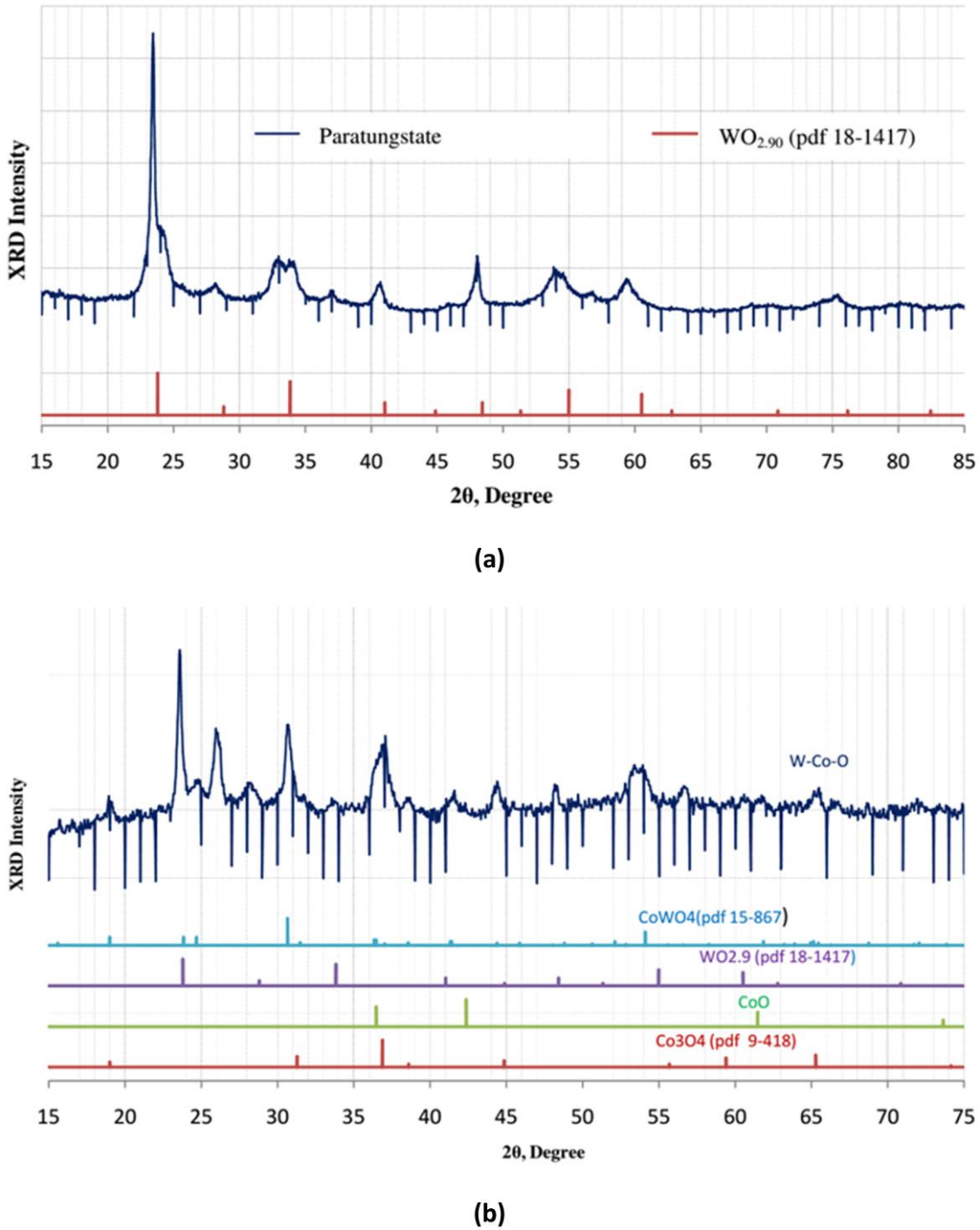

Figure 12 XRD images of (a) tungsten oxide WO_3 obtained by pyrolysis of $(NH_4)_{10}(H_2W_{11}O_{41})\cdot 4H_2O$ at 600°C and (b) tungsten and cobalt oxides obtained by pyrolysis of mixture of $(NH_4)_{10}(H_2W_{11}O_{41})\cdot 4H_2O$, $Co(CH_3COO)_2\cdot 4H_2O$, and $C_{12}H_{22}O_{11}$ of at 600°C.

From a mixture of $(NH_4)_{10}(H_2W_{11}O_{41})\cdot 4H_2O$, $Co(CH_3COO)_2\cdot 4H_2O$, and $C_{12}H_{22}O_{11}$, oxygen-deficient tungsten oxide WO_{3-x}, cobalt oxides CoO and Co_3O_4, $CoWO_4$ phase, and also amorphous carbon are obtained (Figure 12b).

The process of obtaining WO_3 by reducing tungsten to non-stoichiometric oxides with various reductants at relatively low temperatures is well studied. At 800–1000°C, it is reduced to metallic

tungsten in hydrogen flow. It is also possible that the formation of tungsten borides, namely W_2B_5, at low temperatures is due to the interaction of this metal and amorphous boron [93]. Several chemical reactions occur in parallel by heating these preceramic precursors to 1000°C. It was previously established that heat treatment at 800–1000°C in an inert or hydrogen atmosphere produces a mixture of tungsten, cobalt, certain organic compounds, and WC or WC–Co phases. WC–Co was obtained from the mixtures of the compounds used – $(NH_4)_{10}(H_2W_{11}O_{41})\cdot 4H_2O$, $C_{12}H_{22}O_{11}$, WO_3, $Co(CH_3COO)_2\cdot 4H_2O$, and $C_{12}H_{22}O_{11}$ – which is confirmed by XRD structural analysis (Figure 13).

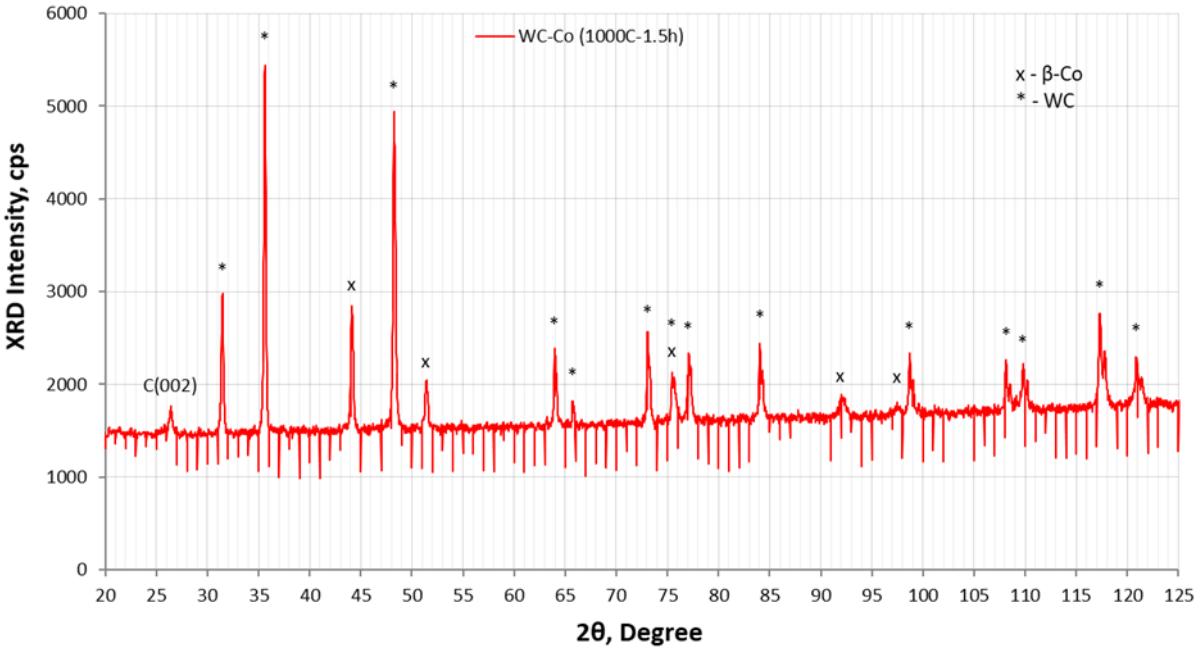

Figure 13 XRD image of WC–Co alloy obtained by thermal decomposition and carbidization of its components from a mixture of WO_3, $Co(CH_3COO)_2\cdot 4H_2O$, and $C_{12}H_{22}O_{11}$.

It is true that the target product could not be obtained by the experiments conducted with Method 1. Still, the development of this method allowed us to get new types of composites, B_4C–TiB_2–W_2B_5 and B_4C–$(Ti,Zr)B_2$–W_2B_5–Co, with exciting properties, which is reflected in the work [94]. B_4C–TiB_2 and WC–Co ultradisperse powders separately synthesized by Method 2 were mixed in a planetary mill using a dry method. The grinding cup and balls were made of hard WC–Co alloy. The duration of mixing did not exceed 6 h, and the speed was 250 rpm. By Method 3, a heterophase system of B_4C–TiB_2-modified WC–Co hard alloy was obtained by mechanical dispersion. Commercial powders of B_4C, TiB_2, and WC–Co (or WC and Co) with a purity of not less than 99.5% were used. The initial powder particle size was ≤5 μm. The dispersion process was carried out using the wet grinding method with a planetary minimill. The grinding cup and balls were made of WC–Co hard alloy. The grinding time was not less than 18 h, and the speed was 250 rpm. The grain size of the dispersed composite was ≤800 nm.

2.3.1 Compaction of WC–Co Alloy Modified with B_4C–TiB_2 Composite by High-Temperature Sintering

As is known, compaction is a technological process that results in a ready-made machine part being obtained from powder. In general, two stages are distinguished: formation and sintering.

However, in some methods, they are combined. Briquettes are often formed by pressing powders at room temperature to obtain bulk products from powders and then sinter them. Among the numerous modern powder metallurgy technologies, uniaxial pressing is the most widespread use for compacting nanopowders. In addition, such pressing can be static (in press forms and tweezers), dynamic (magnetic-impulse and explosion), and vibrational (ultrasonic). However, to obtain high-density samples, a version of the compression method is used, for which the conditions of compression of the material are close to isostatic compression.

We used uniaxial and isostatic pressing methods to form samples for high-temperature grinding. In the samples obtained by uniaxial pressing, stratification and higher porosity are observed in some cases compared to those obtained by isostatic pressing. The so-called shrinkage degree is studied in different directions for isostatically pressed samples. The results of such research are given in Table 3.

Table 3 Dependence of B_4C–30wt.%TiB_2 modifier content in WC–8wt.%Co alloy on shrinkage degree.

#	Sample	State	Width, mm	Height, mm	Length, mm	Volume, mm^3
1	WC–8wt.%Co	Before compacting	5.6	6.8	31.6	1203.3
		After compacting	4.7	5.8	27.0	736.2
		Shrinkage degree	16.0%	14.7%	14.6%	39.0%
2		Before compacting	4.6	6.2	41.6	1186.4
		After compacting	4.0	4.9	35.0	686.0
		Shrinkage degree	13.0%	20.0%	16.0%	42.0%
3	WC–8wt.%Co –10wt.%(B_4C–30wt.%TiB_2) or 83wt.%WC–7wt.%Co –10wt.%(B_4C–30wt.%TiB_2)	Before compacting	6.3	4.6	42.0	1217.1
		After compacting	5.4	4.1	36.7	812.5
		Shrinkage degree	14.0%	11.0%	12.6%	33.0%
4		Before compacting	6.5	6.3	42.0	1720.0
		After compacting	5.8	4.9	38.0	1080.0
		Shrinkage degree	11.0%	22.0%	9.5%	37.2%
5	WC–8wt.%Co –30wt.%(B_4C–30wt.%TiB_2) or 64wt.%WC–6wt.%Co –30wt.%(B_4C–30wt.%TiB_2)	Before compacting	6.1	11.8	41.7	3002.0
		After compacting	5.2	10.3	36.4	1949.5
		Shrinkage degree	14.7%	12.7%	12.7%	35.1%
6		Before compacting	6.3	10.0	42.0	2646.0
		After compacting	5.5	9.1	37.3	1867.0
		Shrinkage degree	12.7%	9.0%	11.2%	29.4%

High-temperature annealing of the samples was carried out in a Taman-type furnace in an argon atmosphere. The annealing temperature was 1430–1460°C, and exposure time was 1.5–2 h. The heating rate up to 1200°C was 20°/min, and from 1200°C to the annealing temperature – 10°/min. The cooling rate was 20°/min. The data in Table 3 show that in the WC–8wt.%Co hard alloy, B_4C–30wt.%TiB_2 modifier content increases, and the shrinkage degree mainly decreases. In general, this

characteristic is determined by the excess free energy property of powder samples, which, in turn, depends on the area of developed surfaces of powders and porous bodies (as sources of excess energy) and the material crystal structure imperfection. The material density, smoothness, electrical conductivity, etc. can evaluate the degree of inter-shrinkage of the components in the composite. In each specific case, this parameter is assessed by the characteristics related to a composite material's function. In our case, the researched sample has higher physical and mechanical characteristics than the BK8 analog. Their values will be given below in Subsections 2.4.2 and 2.4.3.

2.3.2 Compaction of WC–Co Alloy Modified with B_4C–TiB_2 Composite by Spark-Plasma Sintering

Together with the HTS method of compaction, we also selected the SPS method, which allows a much reducing the duration of exposure of the powder material at high temperatures, which in turn leads to the limitation of grain growth and the maximum preservation of the highly dense ultradispersed structure in the compacted samples. As is known, this method is widely used for the compaction of both metallic and non-metallic materials, especially for heterophase ultradispersed and nanomaterials. The SPS method allows a pulsed current to be passed directly into the pre-cold-pressed sample, which produces a high-energy plasma discharge at the particle separation surfaces. SPS is characterized by the cumulative effect of external parameters (pressure and electric current) on its powder compaction and phase formation. However, rapid bulk heating slows down the kinetics of grain size growth. SPS allows the process to be carried out not only with rapid heating but also with fast cooling. Compacting the powder using the SPS method is possible by selecting different options for the characteristic parameters of DC, AC (Alternating Current), and impulse current.

A general view of the used SPS facility is given in Figure 14a. Its chamber (Figure 14b) operates in a vacuum and inert atmosphere. The hydraulic system creates the working pressure. The maximum load is 25 t. The central node of the heating system is a voltage-lowering transformer, which is controlled by an electronic unit. The heating system allows for the passing of AC up to 4000 A in the compaction node. KM54-15 grade graphite is used as a puncher, enabling us to change the working pressure to 100 MPa. Compaction parameters (pressure, sample current, resistance and temperature, punch displacement, etc.) are recorded using a computer block. For consolidation of metal-ceramic samples, special disposable tubes were used, which were made using a mixture of corundum powder and wax. It is more effective to use graphite tubes coated with boron nitride. We covered the graphite with boron nitride using commercial boron nitride aerosols, which have high adhesive properties.

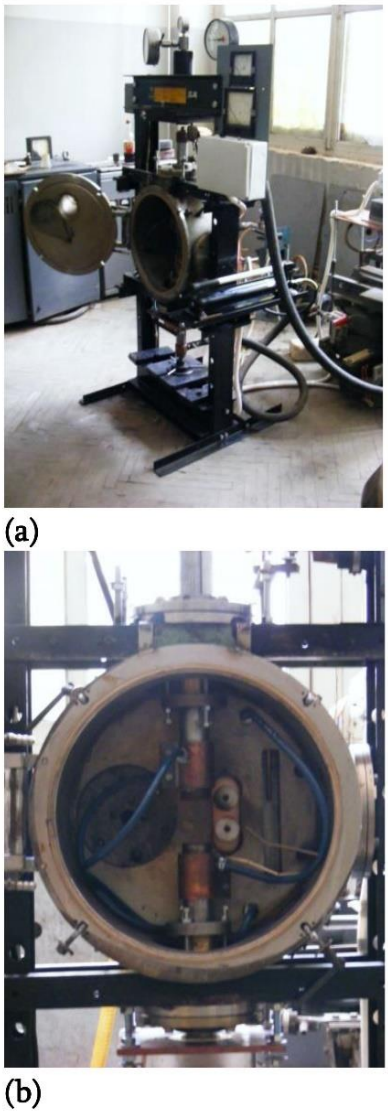

Figure 14 Facility of compaction of electrical current-conducting materials by SPS: (a) general view and (b) chamber.

Compaction using the SPS method is carried out in two steps. In the first step, the current and pressure gradually increase until the melting of the metallic binder (this process is easy to observe because there is a drop in the pressure change curve at the appropriate moment: when the cobalt component in the composite begins to melt, the pressure acting on the sample decreases sharply, which is recorded by the manometer display). The sample is depressurized in the second step and kept at a fixed temperature. The tungsten and tungsten–rhodium W–WRh thermocouple controls the compaction temperature. The compaction temperature around 1500°C is determined by the binder melting temperature.

With this method, we mainly obtained cylindrical samples. Compaction is also possible in prismatic form. However, in this case, a more complex construction of the graphite preform is needed, which will allow us to perform isostatic pressing of the sample and apply the compaction current not in the direction of the axis of the punches, but perpendicular to it – on the bases of the prismatic sample. The main parameters of the process, by which cylindrical samples with a diameter

of 16–30 and a height of 8–15 mm are compacted, are as follows. The compaction temperature is 1500°C, the pressure is 4.5–5.5 MPa, and the duration is 2.5–3 min.

2.4 Structure, Phase Composition, and Physical-Mechanical Properties of Compacted WC–Co Alloy Modified with B_4C–TiB_2 Composite

2.4.1 Structure and Phase Composition of WC–Co–B_4C–TiB_2 Alloy

Both in the multiphase ultradispersed powders obtained from the liquid charges by chemical method and mechanical dispersion, the components are distributed with a high degree of uniformity, which allows for maintaining an even distribution of the component phases in the compacted materials (in the case of both methods of compaction). According to Figure 15 showing the surface of WC–8wt.%Co–30wt.%(B_4C–30wt.%TiB_2) alloy obtained by HTS, all the composite components are ultradispersed and generally uniformly distributed.

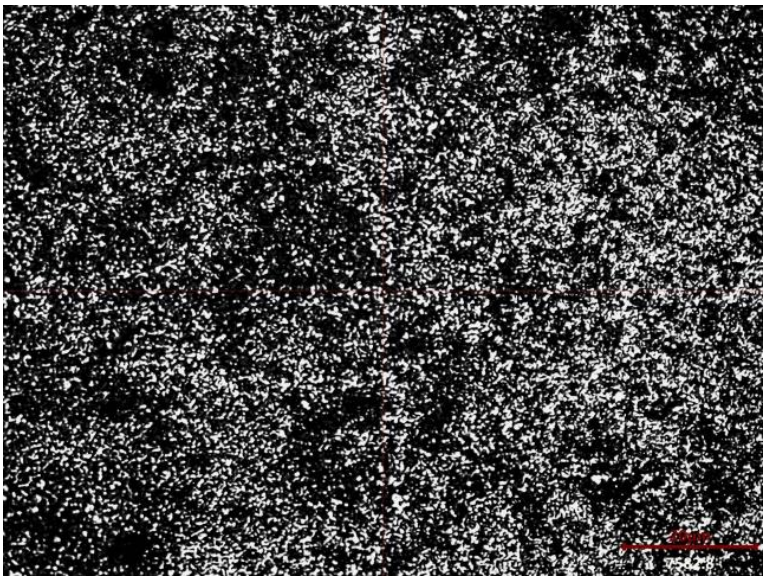

Figure 15 Surface of WC–8wt%Co–30wt%(B_4C–30wt%TiB_2) alloy obtained by HTS.

After compaction by the SPS method, the component phases are fully preserved in the alloys, which is confirmed by their XRD images – see Figure 16.

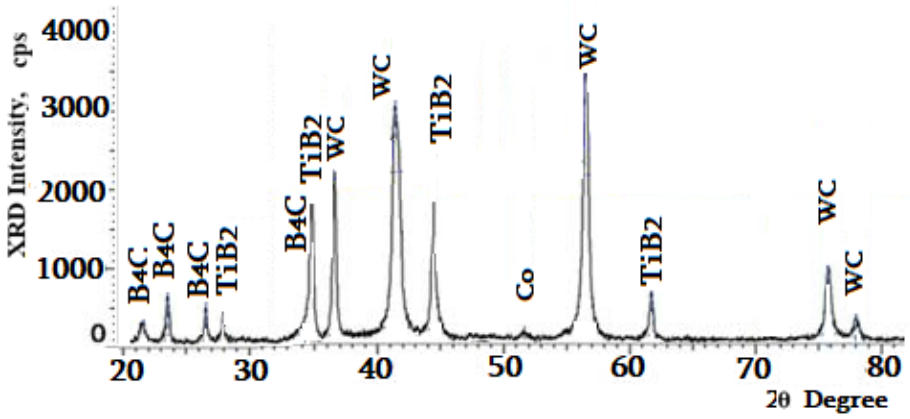

Figure 16 XRD image of WC–8wt.%Co–30wt.%(B_4C–30wt.%TiB_2) alloy.

SEM images, EDX spectra, and wt.% and at.% distributions of chemical elements of the surfaces of alloys of the same composition compacted by HTS and SPS methods are given in Figure 17 and Figure 18, respectively.

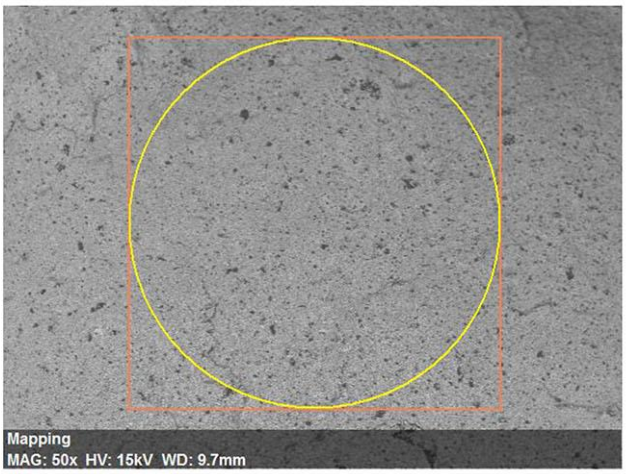

(a)

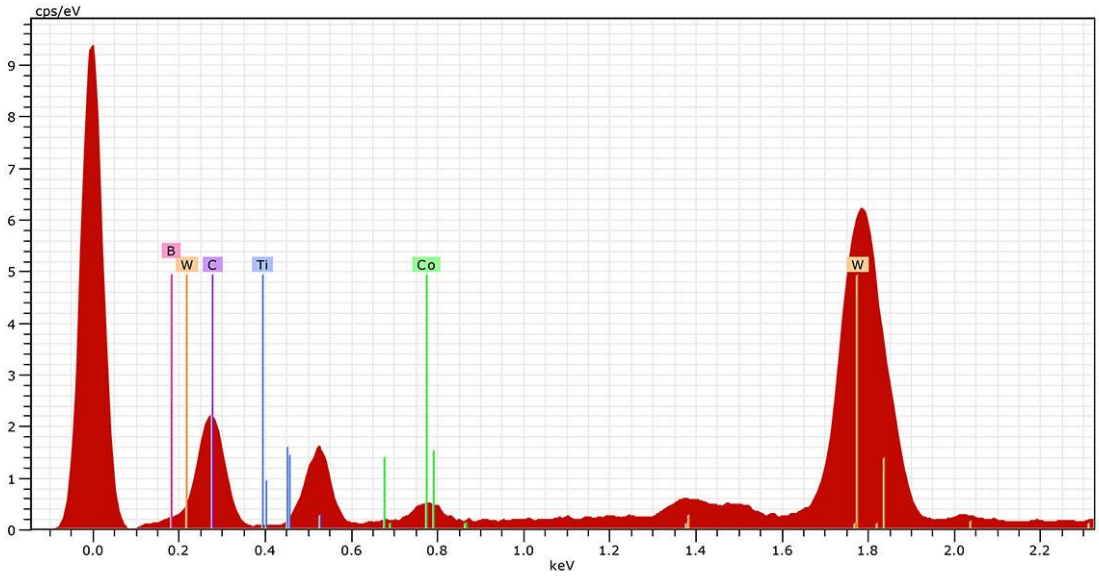

(b)

Chemical element	Series	wt.%	at.%
^{5}B	K	5.77	13.49
^{6}C	K	35.06	73.82
^{22}Ti	K	6.38	3.37
^{27}Co	K	7.05	3.03
^{74}W	L	45.74	6.29
Total	–	100.00	100.00

(c)

Figure 17 SEM image (a), EDX spectrum (b), and chemical elements distribution spectrum analysis results (c) for WC–8wt.%Co–30wt.%(B_4C–30wt.%TiB_2) alloy compacted by HTS.

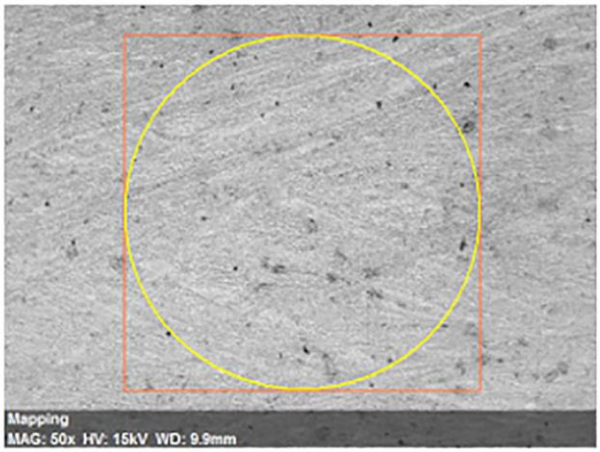

(a)

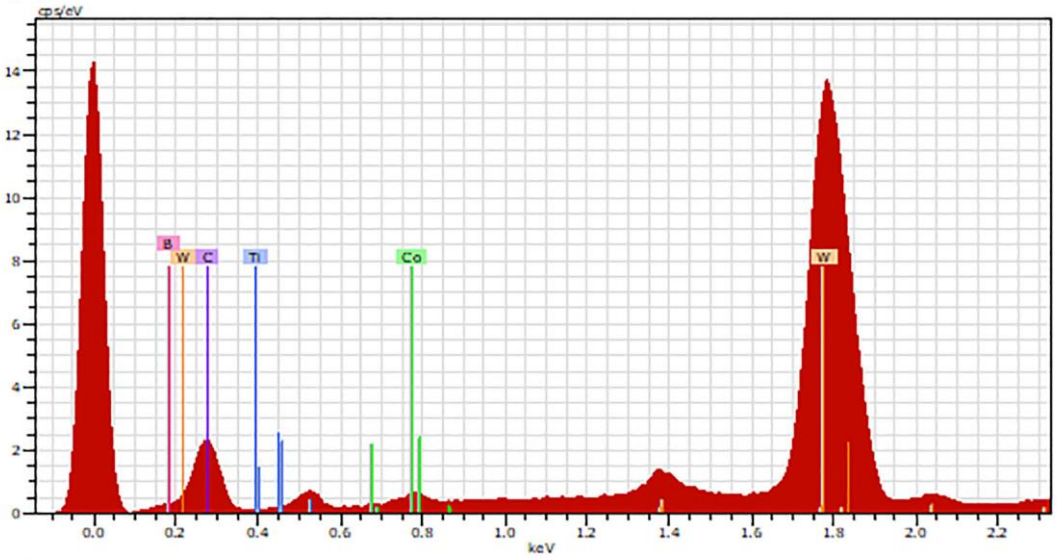

(b)

Chemical element	Series	wt.%	at.%
^{5}B	K	5.81	17.09
^{6}C	K	25.65	67.95
^{22}Ti	K	4.49	2.98
^{27}Co	K	2.43	1.31
^{74}W	L	61.62	10.67
Total	–	100.00	100.00

(c)

Figure 18 SEM image (a), EDX spectrum (b), and chemical elements distribution spectrum analysis results (c) for WC–8wt.%Co–30wt.%(B_4C–30wt.%TiB_2) alloy compacted by SPS.

2.4.2 Hardness of WC–Co–B_4C–TiB_2 Alloy

The hardness of the obtained composite samples is studied depending on component concentration ratios and compaction process parameters.

Table 4 shows the main characteristics of hard alloys of different compositions obtained by dispersion or chemically synthesized and mechanically mixed in an attritor and compacted from these powders by SPS and HTS. Initial powder dispersity was ≤0.8 or ≤0.3 μm, respectively. In all these cases, the matrix was WC–8wt.%Co metal-ceramic, and the modifier was quasieutectic alloy B_4C–30wt.%TiB_2. The highest value of microhardness, 3350 kgf/mm^2, was observed in the WC–8wt.%Co–30wt.%(B_4C–30wt.%TiB_2) composition compacted by SPS method at 1500°C (with initial powder dispersion of ≤0.3 μm). Measurements were carried out on a PMT-3 device under a load of 200 gf.

Table 4 Hardness of WC–8wt.%Co, WC–8wt.%Co–10wt.%(B_4C–30wt.%TiB_2), and WC–8wt.%Co–30wt.%(B_4C–30wt.%TiB_2) alloys depending on dispersion and compacting method.

Initial powder dispersity, μm	Compacting method	Hardness, HRA		
		WC–8wt.%Co	**WC–8wt.%Co –10wt.%(B_4C –30wt.%TiB_2)**	**WC–8wt.%Co –30wt.%(B_4C –30wt.%TiB_2)**
≤0.8	SPS at 1500°C	87.5	89.5	92
		88	90	92.5
		87	90.5	92
≤0.3	SPS at 1500°C	91	92	93
		89	91.5	92
		89.5	91	93
≤0.8	HTS at 1450°C	88	89.5	92
		88	89.5	91.5
		87	90	92
≤0.3	HTS at 1450°C	90	91.5	92
		89	91	91.5
		89	91	92

2.4.3 Bending Strength of WC–Co–B_4C–TiB_2 Alloy

The bending strength σ of WC–Co alloy modified with B_4C–TiB_2 composite, which HTS obtained at a temperature of 1450°C, was determined by so-called the three-point method, i.e. was calculated by the formula $\sigma = 3Wl/2bd^2$, where W [kg] is the breaking load, l [mm] is the distance between the supports – effective length of the sample or "length", b [mm] is the width of the sample (the size in direction perpendicular to the applied force), and d [mm] is its thickness. The mean square deviation S of the results of these measurements was calculated by the formula $S = (\Sigma_i(\sigma_i - \sigma_m)^2/(n-1))^{1/2}$, where σ_i [MPa] is the bending strength of the i-specimen, σ_m [MPa] is the mean of these values. N is the total number of measured samples.

Samples with approximate dimensions of 30 × 5 × 5 mm^3 were used. Their geometric parameters were measured with an accuracy of 0.01 mm. The maximum load on the sample was 505 kgf. The distance between the supports was 18 mm. The rod with which loading is performed was placed in the middle of the supports, at equal distances from them. The results of measuring the bending

strength of the WC–Co metal-ceramic alloy modified with B_4C–TiB_2 ceramic composite are summarized in Table 5.

Table 5 Bending strength of WC–Co alloy modified with B_4C–TiB_2 composite obtained by HTS at temperature of 1450°C in dependence on dispersion and compaction method.

#	Sample	Initial powder dispersity, μm	Load W, kgf	Sample sizes, mm			Bending strength σ, kgf/mm²
				"Length" l, mm	Width b, mm	Thickness d, mm	
1	WC–8wt.%Co	≤0.8	505	18	5.2	4.6	124
2			489	18	5.0	4.6	125
3			433	18	5.1	4.3	124
4		≤0.3	496	18	5.3	4.5	125
5			473	18	5.2	4.4	127
6			504	18	5.0	4.6	129
7	WC–8wt.%Co –10wt.%(B_4C –30wt.%TiB_2)	≤0.8	396	18	4.9	4.5	108
8			390	18	5.1	4.4	107
9			409	18	5.2	4.5	105
10		≤0.3	456	18	5.2	4.6	112
11			393	18	5.0	4.3	115
12			416	18	5.1	4.4	114
13	WC–8wt.%Co –30wt.%(B_4C –30wt.%TiB_2)	≤0.8	397	18	5.3	4.5	100
14			356	18	5.1	4.3	102
15			375	18	5.0	4.5	100
16		≤0.3	420	18	5.1	4.6	105
17			448	18	5.2	4.6	110
18			349	18	5.0	4.3	102

It was not possible to obtain samples with more or less identical geometric sizes because after compaction, the samples needed surface processing and polishing (the samples were processed with diamond disc, and their polishing was done with diamond paste). Specified geometric dimensions of the samples are also shown in Table 5.

Unfortunately, using the SPS method, prismatic shape samples suitable for experimentation could not be obtained, nor could so-called Brinell bending strength k·HB (where k is the coefficient characteristic of a specific material) was theoretically estimated by the measured Brinell hardness HB, because this method is mainly helpful for steels, other metals and metal alloys, and not for relatively fragile metal-ceramics.

3. WC–TiC–Co Alloy Modified with B_4C–TiB_2 Composite

As is known, WC–TiC–Co system alloys of various compositions are widely used in technologies. Such compositions are characterized by high hardness, chemical stability at high temperatures, and wear resistance. The main characteristics of such hard alloys having commercial importance are given in Table 6. Sometimes, these types of alloys are marked with the letters T and K and numbers.

The number after T indicates the wt.% of titanium carbide in the alloy, and K – the cobalt content (meaning the rest is tungsten carbide).

Table 6 Composition and main physical-mechanical characteristics of commercial titanium carbide-containing alloys.

Alloy	Composition, wt.%			Physical-mechanical characteristics		
	WC	TiC	Co	Bending strength, MPa	Density, 10^{-3} kg/m^3	Hardness, HRA
T30K4	66	30	4	≥980	9.5–9.8	≥92
T15K6	79	15	6	≥1176	11.1–11.6	≥90
T14K8	78	14	8	≥1274	11.2–11.6	≥89.5
T5K10	85	6	9	≥1421	12.4–13.1	≥88.5
T5K12	86	5	12	≥1666	13.1–13.5	≥87

In recent years, it has been established that obtaining the powders of these systems in an ultradispersed state and maintaining this state after compaction significantly increases their physical-mechanical and operational characteristics, which are determined by the component ratios. These systems can be obtained in the nanocrystalline state using liquid charge and mechanical-chemical processing. Suppose the composition of the alloy is fixed. In that case, the crucial factors that lead to the increase in the mechanical characteristics of the material are particle size, degree of homogeneity of the structure, and purity of the initial powder. Thus, it is desirable that the sizes of carbide (WC and TiC) powders forming the system should be as small as possible – ultradispersed, and their mixture – homogeneous.

3.1 Obtaining of WC–TiC–Co Alloy Modified with B_4C–TiB_2 Composite

Two standard types of samples, T30K4 (66wt.%WC–30wt.%TiC–4wt.%Co) and T15K6 (79wt.%WC–15wt.%TiC–6wt.%Co), whose hardness values were not less than 92 and 90 HRA, respectively, were studied. Commercial powders of 99.9% WC, TiC, and Co purity were used for the experiments. Separate mechanical dispersion of WC and TiC and then their mixing with Co was carried out in an attritor-type high-energy planetary minimill by the wet method – in the ethyl alcohol medium. By mechanical dispersion, WC–TiC–Co compositions were obtained with approximately the above compositions of standard hard alloys T30K4 and T15K6. The dispersion of the starting materials was reduced to ≤800 nm. These samples were compacted by two methods: the pre-cold-pressed prismatic-shaped samples were compacted by HTS at 1430°C, and the cylindrical-shaped samples were compacted by the SPS method at 1450–1500°C. The XRD image of a sample of T15K6 composition compacted with SPS is given in Figure 19.

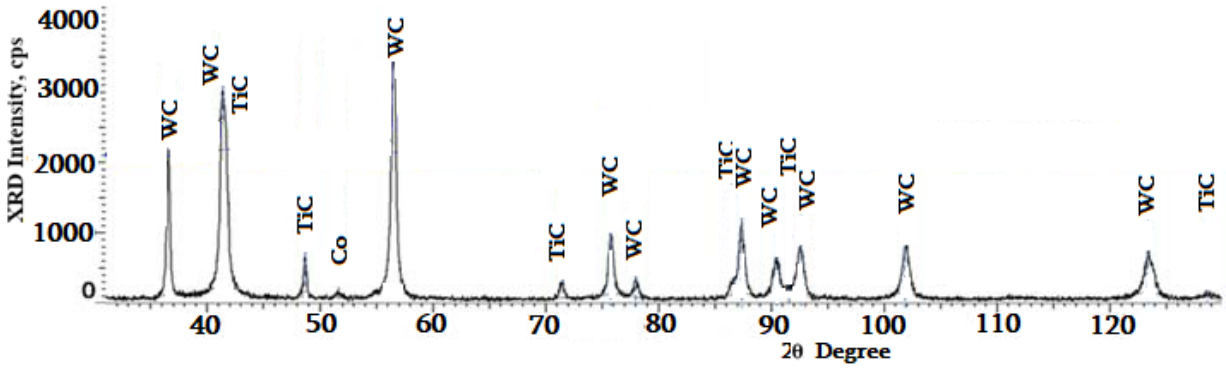

Figure 19 XRD image of T15K6 composition compacted by SPS at temperature of 1450–1500°C.

Composites of the WC–TiC–Co system with the compositions of standard T30K4 and T15K6 hard alloys were obtained by mechanical dispersion. They were modified with B_4C–30wt.%TiB_2 quasieutectic alloy in the following wt.% ratios: (WC–TiC–Co):(B_4C–TiB_2) = 90:10 and 85:15. The wt.% of the components constituting the investigated hard alloys are given in Table 7.

Table 7 Composition of WC–TiC–Co alloy modified with B_4C–TiB_2 composite.

#	Matrix-alloy	Sample	Components wt.%			
			WC	TiC	Co	B_4C–TiB_2
1	T30K4	T30K4–10	59.0	27.0	4.0	10.0
2		T30K4–15	55.7	25.3	4.0	15.0
3	T15K6	T15K6–10	70.6	13.4	6.0	10.0
4		T15K6–15	66.4	12.6	6.0	15.0

The quasieutectic of the B_4C–TiB_2 system was obtained by sintering in an inert atmosphere at 2100°C. The castings were initially crushed in cast iron slabs to a particle size of ≤0.5 mm. Then, the dispersion was continued in the attritor-type planetary mill using the wet method in the area of butyl alcohol. After dispersion, the particle size did not exceed 0.8 µm. Separately dispersed matrix WC–TiC–Co and quasieutectic B_4C–TiB_2 alloys with the appropriate concentration ratios were remixed in an attritor by dry method for 6 h. Compacted samples of alloys of wt.% compositions (WC–TiC–Co):(B_4C–TiB_2) = 90:10 and 85:15 were obtained by HTS and SPS methods, respectively. Their designations are given in Table 7.

3.2 Physical-Mechanical Properties of WC–TiC–Co Alloy Modified with B_4C–TiB_2 Composite

HTS obtained the prism-shaped samples at a temperature of 1460°C in an inert atmosphere during 2 h. Their geometrical sizes, bending strength, and averaged hardness are given in Table 8. Cylindrical-shaped samples were obtained by pressing at 5 MPa and 1450–1500°C for 3 min in an inert atmosphere using the SPS method. After compaction, the phase composition of the T15K6-10 sample was studied using the XRD method. It is established that the phase state is stable during the compaction process, and only the central maxima are recorded on the XRD image (Figure 20). Their averaged hardness characteristics are also given in Table 8.

Table 8 Physical-mechanical characteristics of WC–TiC–Co alloy modified with B_4C–TiB_2 composite.

#	Sample	Load W, kgf	Sample sizes, mm			Bending strength, kgf/mm^2	Mean hardness, HRA
			l	b	d		
1	T30K4–10wt.%(B_4C–TiB_2)	397	18	5.2	4.6	97	92.0
2		387	18	5.0	4.6	99	
3		404	18	5.0	4.7	99	
4	T30K4–15wt.%(B_4C–TiB_2)	386	18	5.1	4.5	101	92.3
5		426	18	5.0	4.8	100	
6		412	18	5.1	4.7	99	
7	T15K6–10wt.%(B_4C–TiB_2)	506	18	5.2	4.7	119	91.2
8		469	18	5.0	4.6	120	
9		471	18	5.2	4.5	121	
10	T15K6–15wt.%(B_4C–TiB_2)	459	18	5.1	4.6	115	91.5
11		488	18	5.1	4.7	117	
12		460	18	5.2	4.5	118	

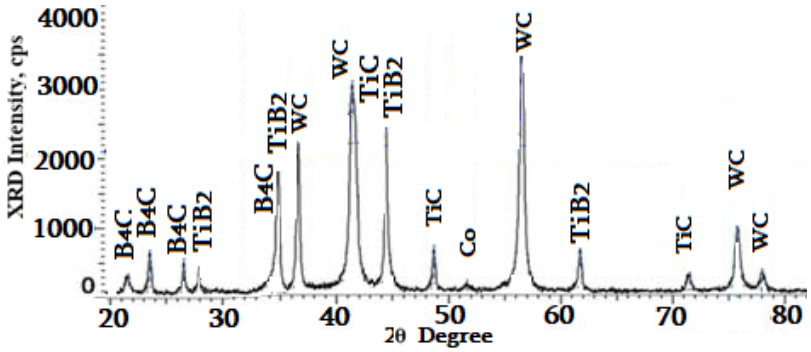

Figure 20 XRD image of T15K6-10 alloy modified with B_4C–TiB_2 composite.

When measuring the microhardness of the (WC–TiC–Co)–(B_4C–TiB_2) samples, the highest value, 2993 kgf/mm^2, was observed in the T30K4–15wt.%(B_4C–TiB_2) sample compacted by the SPS method at 1450–1500°C. Its initial powder dispersion was ≤0.8 μm. Measurements were done on PMT–3 devices under 200 gf load conditions.

Compacted samples of (WC–TiC–Co):(B_4C–30wt.%TiB_2) = 90:10 and 85:15 wt.% composition alloys were obtained by HTS and SPS methods, respectively. Figure 21 presents the SEM image of T15K6–10wt.%(B_4C–30wt.%TiB_2) hard alloy obtained by HTS and the corresponding EDX spectrum with wt.% and at.% distribution of chemical elements.

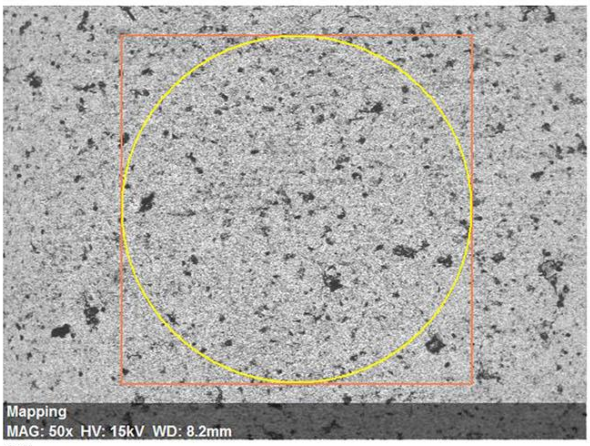

(a)

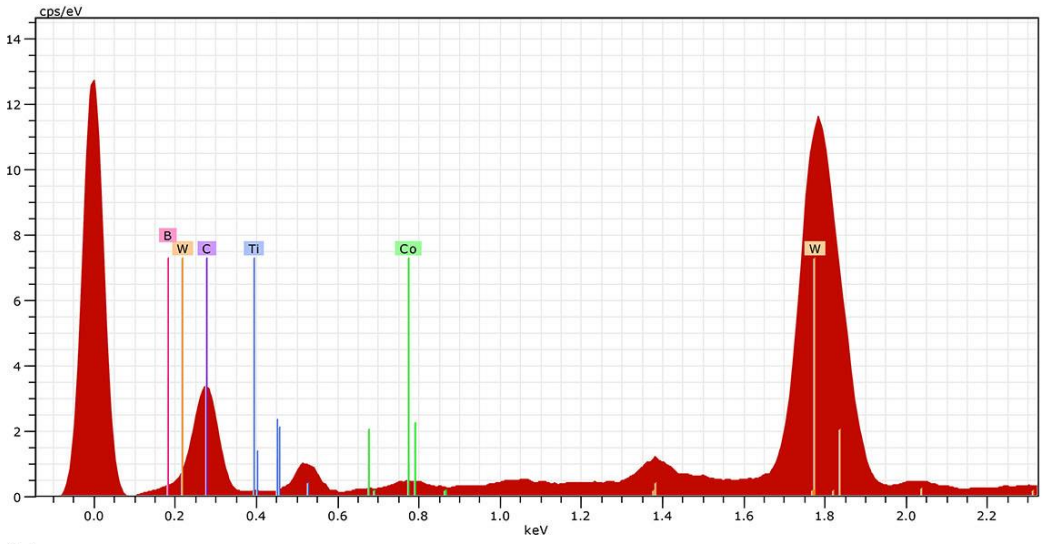

(b)

Chemical element	Series	wt.%	at.%
^{5}B	K	4.60	11.94
^{6}C	K	32.38	75.66
^{22}Ti	K	4.91	2.88
^{27}Co	K	1.99	0.95
^{74}W	L	56.12	8.57
Total	–	100.00	100.00

(c)

Figure 21 SEM image (a), EDX spectrum (b), and chemical elements distribution spectrum analysis results (c) for T15K6–10wt.%(B_4C–30wt.%TiB_2) alloy.

4. Utilization of W-containing Scrap by Treatment with Hydrogen Peroxide

Scraps of tungsten heaters of different diameters were used for the utilization of tungsten-containing waste. Utilization was carried out at room temperature using highly concentrated (30%) hydrogen peroxide, in which the tungsten scrap was dissolved entirely and a true solution was obtained. Tungsten forms compounds with hydrogen peroxide, so-called supertungstates, pertungstates, or tungsten peroxides, which are well soluble in water, stable enough in low-

temperature aqueous solutions, and help to establish equilibrium between a pertungstate and hydrogen peroxide.

Using a pertungstate aims to prepare ultradispersed tungsten carbide-based liquid charges to obtain hard alloys. For this, tungsten or pertungstate is dissolved in hydrogen peroxide and aqueous solutions of cobalt acetate $Co(CH_3COO)_3$ and sucrose $C_{12}H_{22}O_{11}$. By dehydrating the mixture at 150–200°C and then by two-step heat treatment of the resulting powder mass in an inert atmosphere at temperatures of 600 and 950–1000°C for 2.5 and 1.5 h, respectively, WC–Co powder alloy in ultradispersed form is obtained. The phase formation process in WC–Co alloy at temperatures of 800 and 1000°C is studied using the XRD method. As the analysis shows, cobalt and tungsten oxides and free tungsten and carbon are detected at 800°C in the composite together with main phases (WC and Co). This shows that the reduction processes of metals from corresponding oxides and their carbonization are not completed under the given conditions. They are finished only at 1000°C with the formation of the target product – WC–Co alloy.

The problem of utilization of tungsten scrap, i.e., secondary processing, arose along with the creation of tungsten products. The reason for this can be easily explained: the majority of tungsten deposits contain up to 1% of tungsten, which is usually in the form of WO_3 oxide, while the amount of tungsten in the slurry obtained by mining with tungsten tools is, on average 15 times higher than the mentioned concentration. On the other hand, the demand for tungsten in various industry sectors is increasing daily. This is why methods of extraction of tungsten from tungsten-containing scrap have been intensively developed for ten years.

In the last part of the literature review of this article, the main ways and methods of utilization of tungsten-containing scrap were discussed. Special attention is paid to the economy and environmental friendliness of such methods. Here, we present the preliminary work conducted to study the processes of utilizing tungsten-containing scrap and waste and to determine the possibility of obtaining tungsten-containing complex composites from the materials obtained by using scarp.

Scraps of tungsten heaters of different diameters were used for the utilization of tungsten-containing waste. The utilization process was carried out at room temperature using highly concentrated (30%) hydrogen peroxide to dissolve the tungsten scrap and ultimately obtain a true solution. Tungsten forms compounds, such as supertungstates and pertungstates, which are yellow and dissolve well in water. They are stable enough in aqueous solutions even at low temperatures and establish equilibrium with hydrogen peroxide. An uncolored pertungstate is also obtained, spontaneously formed from yellow in a moist environment within 1–2 days. The behavior of white pertungstate for water does not differ from that of yellow—dehydration of pertungstate and subsequent heat treatment at 600°C yields tungsten oxide WO_3.

Both products obtained from tungsten scrap are widely used in the chemical industry. To obtain hard alloys, we aimed to create a tungsten carbide-based liquid charge in an ultradispersed state. We used tungsten dissolved in hydrogen peroxide, a so-called pertungstate solution, and mixtures of aqueous solutions of cobalt acetate $Co(CH_3COO)_3$, and sucrose. By dehydrating the mixture at 150–200°C and then thermally treating the resulting powder mass in an inert atmosphere in steps of 600°C (2.5 h) and 950–1000°C (1.5 h), an ultradispersed alloy of powdered WC–Co was obtained.

The formation process of WC–Co alloy at 800°C was studied by XRD structural analysis. It can be seen that the phase formation process is not completed at the mentioned temperature because cobalt and tungsten oxides and free tungsten and carbon are presented together with the

composite main components, WC and Co. This shows that the processes of reduction of metals from oxides and their carbonization could not be finished under given conditions. Intermediate phases are represented in the XRD image (Figure 22a).

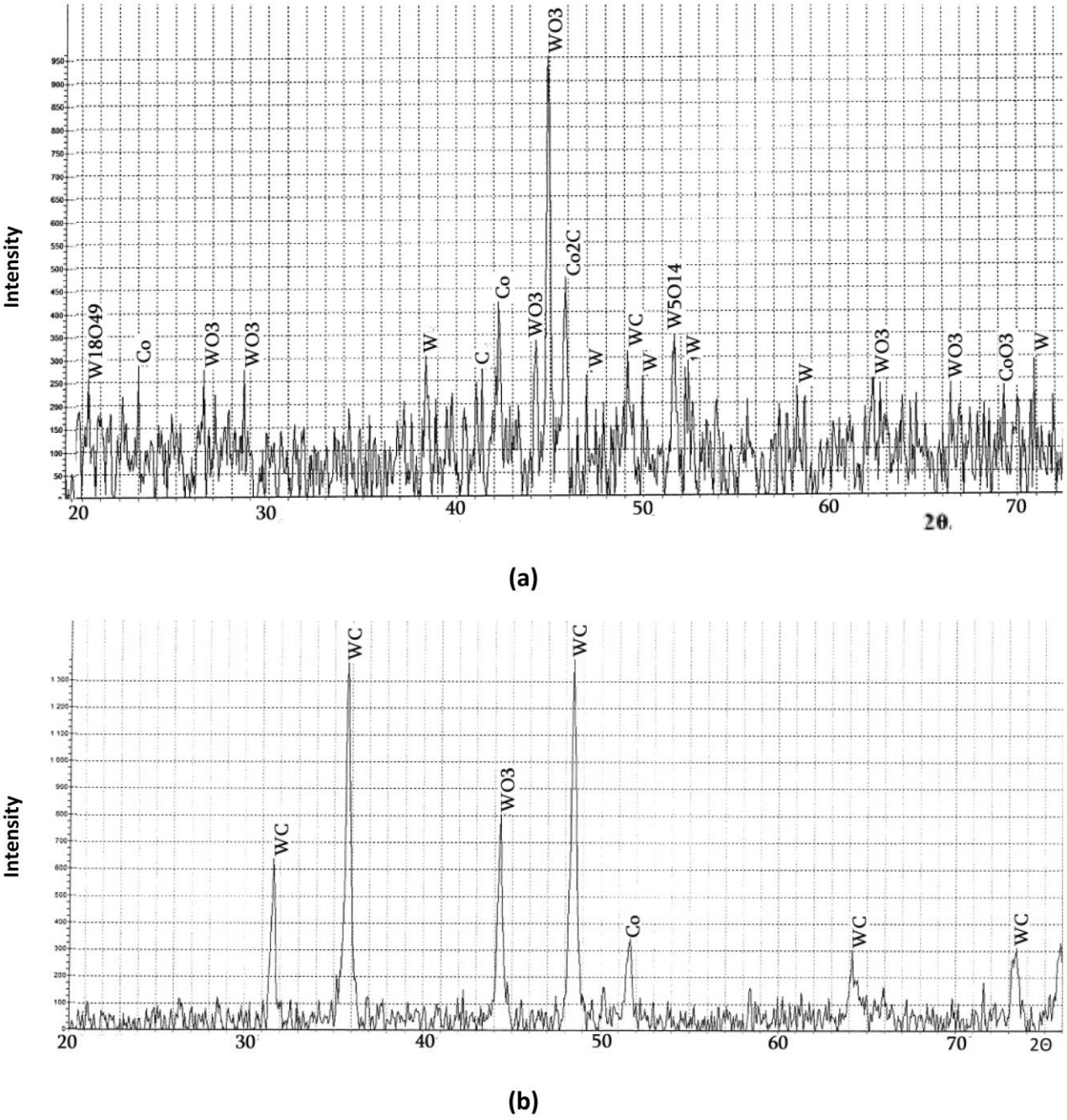

Figure 22 XRD images of WC–Co alloy obtained from the liquid charge of a mixture of pertungstate, cobalt acetate, and sucrose aqueous solutions by heat treatment at (a) 800 and (b) 1000°C.

By increasing the processing temperature to 1000°C, a WC–Co alloy is obtained. Residual tungsten oxide is also observed on the XRD image, which should be related to carbon deficiency in the charge (Figure 22b). Compaction of the obtained WC–Co powder alloy was carried out by the high-temperature annealing method at 1450°C with a duration of 1.5 h. The phase composition of

the obtained WC–Co hard alloy is approximately the same as that of the standard BK8 grade (in our case, the cobalt content is approximately 7.6wt.%).

5. Conclusions

The basic component of the hard composite materials studied here is tungsten carbide WC, its mechanical mixture with titanium carbide WC–TiC, and metallic cobalt Co, the binder for cementing such ceramic matrix particles. As for the quasieutectic alloy of boron carbide–titanium diboride, B_4C–30wt.%TiB_2 acts as a composite modifier. In this modifier, the share of boron carbide B_4C as the main component is 70wt.%, while titanium diboride TiB_2 with a share of 30wt.% is its additive.

By mechanically dispersing commercial powders of B_4C and TiB_2 in an attritor, quasieutectic alloy (of wt.% composition B_4C:TiB_2 = 70:30) with a degree of dispersion of ≤0.8 μm was obtained. The same alloy is obtained using a liquid charge (suspended aqueous solution of titanium dioxide, amorphous boron, and sucrose). By dehydrating it at 100–110°C and step-wise heat treatment of the obtained mass at temperatures of 600–800 and 1250–1300°C, a powder with a particle size of ≤0.8 μm was formed.

WC–Co alloy was also synthesized by a chemical method using various liquid phases (tungsten and cobalt chlorides and neurotrophin, as well as ammonium paratungstate, cobalt acetate, and sucrose aqueous solutions) and the phase formation process was studied by XRD method in the temperature range of 750–1000°C. The particle size of the powders obtained from both charges did not exceed 0.3 μm.

Ammonium paratungstate, titanium dioxide, cobalt acetate, sucrose, and amorphous boron were selected as precursor components for the formation of WC–B_4C–TiB_2–Co ultradispersed system in a single process using the chemical method, and the charge was obtained in the form of paste. Its thermal treatment was carried out at the temperature necessary to obtain tungsten carbide WC (not less than 1000°C). W_2B_5 phase of tungsten boride was formed in the system instead of target WC. The experiments in frames of this version of the obtaining method did not yield the target product. Still, they allowed us to develop new types of heterophase ceramic and metal-ceramic composites B_4C–TiB_2–W_2B_5 and B_4C–$(Ti,Zr)B_2$–W_2B_5–Co with exciting properties.

The materials of two groups of hard alloys modified with quasieutectic alloy B_4C–TiB_2 of different concentration-compositions, WC–Co (BK8) and WC–TiC–Co (T30K4 and T15K6), were obtained by chemical method and mechanical dispersion in attritor and studied. The particle size of composite powders obtained by the chemical method was ≤0.3 μm, and those obtained by mechanical dispersion were ≤0.8 μm. The compaction of metal-ceramic composite powders is carried out using SPS and HTS methods.

Among the obtained samples, two samples are characterized by high hardness and satisfactory bending strength. From the WC–Co (BK8) group, these are WC–8wt.%Co–30wt.%(B_4C–30wt.%TiB_2) alloys, the components of which are obtained by chemical method. The grain size was ≤0.3 μm. When the samples are compacted by the SPS method at a temperature of 1500°C and pressure of 5 MPa, their average parameters are hardness 93.0 HRA and microhardness 3350 kgf/mm^2. Moreover, for samples compacted by HTS: the hardness is 92.0 kgf/mm^2 and the bending strength is 106 kgf/mm^2. When WC–TiC–Co (T30K4) group WC–30wt.%TiC–4wt.%Co–15wt.%(B_4C–30wt.%TiB_2) alloy components obtained by mechanical dispersion of powders (particles with size

≤0.8 μm) were compacted by HTS at temperature of 1450°C, the samples have hardness of 92.3 HRA, a microhardness of 2993 kgf/mm^2, and bending strength of 100 kgf/mm^2.

Preliminary work was carried out to study the utilization processes of tungsten-containing scrap and waste and to determine the possibilities of obtaining tungsten-containing complex composites from recycled materials. Utilization of tungsten scrap (heaters waste) was carried out using highly concentrated (30%) hydrogen peroxide at room temperature. The WC–Co alloy was synthesized with tungsten from such liquid charge.

Author Contributions

Dr. Otar Tsagareishvili: conceptualization, investigation, methodology, project administration, resources, visualization, writing – original draft. Dr. Archil Mikeladze: formal analysis, investigation, validation, visualization. Dr. Roin Chedia: conceptualization, formal analysis, investigation, methodology, validation, visualization. Dr. Tamaz Batsikadze: formal analysis, investigation, validation, visualization. Prof. Dr. Levan Chkhartishvili: conceptualization, data curation, investigation, methodology, supervision, visualization, writing – original draft, writing – review and editing. All authors have read and approved the published version of the manuscript.

Competing Interests

The authors have declared that no competing interests exist.

References

1. Sharshir S, El-Attar H, Basem A, El-Naggar AA, Alaraj AM, Attia A, et al. An overview of the progress in the synthesis of nanocomposites for industrial applications: Techniques preparation, definitions, and characterization. Synth Met. 2024; 307: 117665.
2. Silvestroni L, Kleebe HJ, Fahrenholtz WG, Watts J. Super-strong materials for temperatures exceeding 2000°C. Sci Rep. 2017; 7: 40730.
3. Sharapova VA. Special Composite Materials. Ekaterinburg, Russia: Ural University Press; 2020.
4. Fang ZZ, Wang X, Ryu T, Hwang KS, Sohn HY. Synthesis, sintering, and mechanical properties of nanocrystalline cemented tungsten carbide–A review. Int J Refract Met Hard Mater. 2009; 27: 288-299.
5. Fernandes CM, Senos AM. Cemented carbide phase diagrams: A review. Int J Refract Met Hard Mater. 2011; 29: 405-418.
6. Panov VS. Nanostructured sintered WC–Co hard metals. Powder Metall Met Ceram. 2015; 53: 643-654.
7. Kataria R, Kumar J. Machining of WC-Co composites-A review. Mater Sci Forum. 2015; 808: 51-64.
8. Bobzin K. High-performance coatings for cutting tools. CIRP J Manuf Sci Technol. 2017; 18: 1-9.
9. Zhang J, Saeed MH, Li S. Recent progress in development of high-performance tungsten carbide-based composites: Synthesis, characterization, and potential applications. In: Advances in ceramic matrix composites. Woodhead Publishing; 2018. pp. 307-329.

10. Farag S, Konyashin I, Ries B. The influence of grain growth inhibitors on the microstructure and properties of submicron, ultrafine and nano-structured hardmetals–A review. Int J Refract Met Hard Mater. 2018; 77: 12-30.
11. Sun J, Zhao J, Gong F, Ni X, Li Z. Development and application of WC-based alloys bonded with alternative binder phase. Crit Rev Solid State Mater Sci. 2019; 44: 211-238.
12. Bhadauria G, Jha SK, Roy BN, Dhakry NS. Electrical-discharge machining of tungsten carbide (WC) and its composites (WC-Co)–A review. Mater Today Proc. 2018; 5: 24760-24769.
13. García J, Ciprés VC, Blomqvist A, Kaplan B. Cemented carbide microstructures: A review. Int J Refract Met Hard Mater. 2019; 80: 40-68.
14. Cha SI, Hong SH, Kim BK. Spark plasma sintering behavior of nanocrystalline WC–10Co cemented carbide powders. Mater Sci Eng A. 2003; 351: 31-38.
15. Kim HC, Shon IJ, Yoon JK, Doh JM. Consolidation of ultra fine WC and WC–Co hard materials by pulsed current activated sintering and its mechanical properties. Int J Refract Met Hard Mater. 2007; 25: 46-52.
16. Zhao S, Song X, Zhang J, Liu X. Effects of scale combination and contact condition of raw powders on SPS sintered near-nanocrystalline WC–Co alloy. Mater Sci Eng A. 2008; 473: 323-329.
17. Liu W, Song X, Wang K, Zhang J, Zhang G, Liu X. A novel rapid route for synthesizing WC–Co bulk by in situ reactions in spark plasma sintering. Mater Sci Eng A. 2009; 499: 476-481.
18. Mannesson K, Borgh I, Borgenstam A, Ågren J. Abnormal grain growth in cemented carbides—Experiments and simulations. Int J Refract Met Hard Mater. 2011; 29: 488-494.
19. Falkovsky VA, Klyachko LI, Glushkov VN, Khokhlov AM, Eiduk ON, Lukashova NM. Multi-carbide hardmetals. In: 15th International Plansee Seminar 2001–Powder Metallurgical High Performance Materials, Volume 2: P/M Hard Materials. Reutte, Austria: Plansee Holding AG; 2011. Available from: https://inis.iaea.org/collection/NCLCollectionStore/_Public/32/068/32068438.pdf.
20. Falkovsky V, Glushkov V, Klyachko L, Khokhlov A, Blagoveschenski Y. Nanocrystalline WC-Co hardmetals produced by plasmochemical method. In: 15th International Plansee Seminar 2001–Powder Metallurgical High Performance Materials, Volume 2: P/M Hard Materials. Reutte, Austria: Plansee Holding AG; 2011. Available from: https://inis.iaea.org/collection/NCLCollectionStore/_Public/32/068/32068438.pdf.
21. Rui BA, Yi JH, Peng YD, Zhang HZ, Li AK. Decarburization and improvement of ultra fine straight WC–8Co sintered via microwave sintering. Trans Nonferrous Met Soc China. 2012; 22: 853-857.
22. Wei CB, Song XY, Fu J, Liu XM, Gao Y, Wang HB, et al. Microstructure and properties of ultrafine cemented carbides—Differences in spark plasma sintering and sinter-HIP. Mater Sci Eng A. 2012; 552: 427-433.
23. Xiao TD, Tan X, Yi M, Peng S, Peng F, Yang J, et al. Synthesis of commercial-scale tungsten carbide-cobalt (WC/Co) nanocomposite using aqueous solutions of tungsten (W), cobalt (Co), and carbon (C) precursors. J Mater Sci Chem Eng. 2014; 2: 47605.
24. Chang SH, Chang MH, Huang KT. Study on the sintered characteristics and properties of nanostructured WC–15 wt%(Fe–Ni–Co) and WC–15 wt% Co hard metal alloys. J Alloys Compd. 2015; 649: 89-95.
25. Wang H, Webb T, Bitler JW. Study of thermal expansion and thermal conductivity of cemented WC–Co composite. Int J Refract Met Hard Mater. 2015; 49: 170-177.

26. Efimovich IA, Zolotukhin IS, Zav'alov ES. Thermal coefficient of linear expansion of tungsten–Cobalt cemented carbide. Met Work Mater Sci. 2019; 21: 129-140.
27. Rumman MR, Xie Z, Hong SJ, Ghomashchi R. Effect of spark plasma sintering pressure on mechanical properties of WC–7.5 wt% Nano Co. Mater Des. 2015; 68: 221-227.
28. Raihanuzzaman RM, Rosinski M, Xie Z, Ghomashchi R. Microstructure and mechanical properties and of pulse plasma compacted WC-Co. Int J Refract Met Hard Mater. 2016; 60: 58-67.
29. Yang Q, Yang J, Yang H, Ruan J. The effects of fine WC contents and temperature on the microstructure and mechanical properties of inhomogeneous WC-(fine WC-Co) cemented carbides. Ceram Int. 2016; 42: 18100-18107.
30. Su W, Huang Z, Ren X, Chen H, Ruan J. Investigation on morphology evolution of coarse grained WC–6Co cemented carbides fabricated by ball milling route and hydrogen reduction route. Int J Refract Met Hard Mater. 2016; 56: 110-117.
31. Lin H, Sun J, Li C, He H, Qin L, Li Q. A facile route to synthesize WC–Co nanocomposite powders and properties of sintered bulk. J Alloys Compd. 2016; 682: 531-536.
32. Liu K, Wang Z, Yin Z, Cao L, Yuan J. Effect of Co content on microstructure and mechanical properties of ultrafine grained WC-Co cemented carbide sintered by spark plasma sintering. Ceram Int. 2018; 44: 18711-18718.
33. He M, Wang J, He R, Yang H, Ruan J. Effect of cobalt content on the microstructure and mechanical properties of coarse grained WC-Co cemented carbides fabricated from chemically coated composite powder. J Alloys Compd. 2018; 766: 556-563.
34. Wang B, Wang Z, Yin Z, Liu K, Yuan J. Effects of powder preparation and sintering temperature on consolidation of ultrafine WC-8Co tool material produced by spark plasma sintering. Ceram Int. 2019; 45: 19737-19746.
35. Ruziev UN, Guro VP, Safarov YT, Rasulova SN. Doping of hard alloy VK-6 with vanadium carbide. Chem Solid State (in Russian). 2019; 8: 1-4. Available from: https://cyberleninka.ru/article/n/legirovanie-tverdogo-splava-vk-6-karbidom-vanadiya.
36. Yang Y, Zhang C, Wang D, Nie L, Wellmann D, Tian Y. Additive manufacturing of WC-Co hardmetals: A review. Int J Adv Manuf Technol. 2020; 108: 1653-1673.
37. Ke Z, Zheng Y, Zhang G, Wu H, Xu X, Lu X, et al. Fabrication of dual-grain structure WC-Co cemented carbide by in-situ carbothermal reduction of WO_3 and subsequent liquid sintering. Ceram Int. 2020; 46: 12767-12772.
38. He R, Li B, Ou P, Yang C, Yang H, Ruan J. Effects of ultrafine WC on the densification behavior and microstructural evolution of coarse-grained WC-5Co cemented carbides. Ceram Int. 2020; 46: 12852-12860.
39. Goncharuk VA. Influence of structural factors on the mechanical properties of high-strength composite materials based on refractory compounds [Internet]. Kyiv, Ukraine: I. M. Frantsevich Institute for Problems of Materials Science of the NAS of Ukraine; 2021. Available from: http://www.materials.kiev.ua/abstract/67/Autoref_Goncharuka.pdf.
40. Pereira P, Vilhena LM, Sacramento J, Senos AM, Malheiros LF, Ramalho A. Abrasive wear resistance of WC-based composites, produced with Co or Ni-rich binders. Wear. 2021; 482: 203924.

41. Wachowicz J, Dembiczak T, Stradomski G, Bałaga Z, Dyner M, Wilkowski J. Properties of WCCo composites produced by the SPS method intended for cutting tools for machining of wood-based materials. Materials. 2021; 14: 2618.
42. Ye Y, Xia H, Lin Y, Chen F, Shen Q. Refined WC grain size and improved mechanical properties in a hardmetal WC-8Co processed via short-time semi-solid hot pressing. J Alloys Compd. 2021; 889: 161560.
43. Buravleva AA, Fedorets AN, Vornovskikh AA, Ognev AV, Nepomnyushchaya VA, Sakhnevich VN, et al. Spark plasma sintering of WC-based 10wt% Co hard alloy: A study of sintering kinetics and solid-phase processes. Materials. 2022; 15: 1091.
44. Soria-Biurrun T, Lozada-Cabezas L, Navarrete-Cuadrado J, Ibarreta-Lopez F, Martinez-Pampliega R, Sánchez-Moreno JM. Densification of WC-Fe-Ni-Co-Cr cemented carbides processed by HIP after sintering: Effect of WC powder particle size. Int J Refract Met Hard Mater. 2023; 110: 105994.
45. Li X, Zhang J, Zhang Q, Zhang X, Ji V, Liu J. Microstructure evolution and hardness improvement of WC-Co composites sintered with fe substituting part of Co binder. Coatings. 2023; 13: 116.
46. Tanaka Y, Sato H, Eryu O. Structural modification of WC-Co cutting tools by laser doping treatment. Heliyon. 2023; 9: e19930.
47. Teslia SY, Kucher OS, Bogomol II, Loboda PI, Solodkyi IV. Induction zone sintering of WC–8Co hard alloy. Mater Sci. 2024; 59: 638-643.
48. Kim HC, Kim DK. Sintering behavior and mechanical properties of binderless WC-TiC produced by pulsed current activated sintering. J Ceram Process Res. 2007; 8: 91-97.
49. Kim HC, Kim DK, Woo KD, Ko IY, Shon IJ. Consolidation of binderless WC–TiC by high frequency induction heating sintering. Int J Refract Met Hard Mater. 2008; 26: 48-54.
50. Dash T, Nayak BB. Tungsten carbide–Titanium carbide composite preparation by arc plasma melting and its characterization. Ceram Int. 2019; 45: 4771-4780.
51. Yoon BK, Lee BA, Kang SJ. Growth behavior of rounded (Ti,W) C and faceted WC grains in a Co matrix during liquid phase sintering. Acta Mater. 2005; 53: 4677-4685.
52. Lee KH, Cha SI, Kim BK, Hong SH. Effect of WC/TiC grain size ratio on microstructure and mechanical properties of WC–TiC–Co cemented carbides. Int J Refract Met Hard Mater. 2006; 24: 109-114.
53. Ha GH, Lee GG, Yang MC, Kim BK. Synthesis of WC–TiC–Co nanopowder by mechano-chemical process. In: European PM Conference Proceedings. Chantilly, France: The European Powder Metallurgy Association; 2006. pp. 97-102.
54. Song J, Huang C, Zou B, Liu H, Liu L, Wang J. Effects of sintering additives on microstructure and mechanical properties of TiB_2–WC ceramic–metal composite tool materials. Int J Refract Met Hard Mater. 2012; 30: 91-95.
55. Zhang CC, Wang Q, Yuan QQ, Yang YF, Yi XL. Preparation of WC-5TiC-10Co nanometer powder and performance study of sintering samples. Adv Mater Res. 2012; 465: 220-223.
56. Chen J, Gong MF, Wu SH. Flank wear mechanism of WC-5TiC-10Co cemented carbides inserts when machining HT250 gray cast iron. Appl Mech Mater. 2014; 670: 517-521.
57. Dutkiewicz J, Bobrowski P, Szutkowska M, Leniewski W, Duzews P. The effect of substitution of WC by TiC in WC-Co composite tool materials on microstructure and mechanical properties. Chiang Mai J Sci. 2017; 44: 1714-1721.

58. Bogodukhov SI, Kozik ES, Svidenko EV. Thermal hardening of hard alloy T15K6. Ind Lab Diagn Mater. 2017; 83: 38-42.
59. Zhang C, Song J, Jiang L, Gao J, Liang G, Lei C, et al. Fabrication and tribological properties of WC-TiB_2 composite cutting tool materials under dry sliding condition. Tribol Int. 2017; 109: 97-103.
60. Zhao SC, Liu N, Chen AH. Effect of titanium carbide on microstructure and properties of fine grain WC-13Co cemented carbides. Trans Mater Heat Treat. 2018; 39: 45-50.
61. Szutkowska M, Boniecki M, Cygan S, Kalinka A, Grilli ML, Balos S. Fracture behaviour of WC-Co hardmetals with WC partially substituted by titanium carbide. IOP Conf Ser Mater Sci Eng. 2018; 329: 012015.
62. Bouleghlem M, Zahzouh M, Hamidouche M, Boukhobza A, Fellah M. Microstructural and mechanical investigation of WC-TiC-Co cemented carbides obtained by conventional powder metallurgy. Int J Eng Res Afr. 2019; 45: 1-14.
63. Kacmaz D, Kalkavan F, Yazıcı S, Demirural A, Baykara T. Processing, sintering and performance of WC–Co-near-nano-TiC metal matrix composites. Res Dev Mater Sci. 2019; 9: 1012-1018.
64. Zhou H, Wang Z, Wang B. Fabrication of WC-Co/(Ti,W) C graded cemented carbide by spark plasma sintering. Int J Refract Met Hard Mater. 2020; 87: 105141.
65. Chen J, Zhou L, Liang J, Liu B, Liu J, Chen R, et al. Effect of initial WC particle size on grain growth behavior and gradient structure formation of bilayer functionally graded cemented carbides. Mater Chem Phys. 2021; 271: 124919.
66. Buravlev IY, Shichalin OO, Papynov EK, Golub AV, Gridasova EA, Buravleva AA, et al. WC-5TiC-10Co hard metal alloy fabrication via mechanochemical and SPS techniques. Int J Refract Met Hard Mater. 2021; 94: 105385.
67. Ke Z, Zheng Y, Zhang G, Zhang J, Wu H, Xu X, et al. Microstructure and mechanical properties of WC-(Ti,W) C-Co hardmetals fabricated by in-situ carbothermal reduction of oxides and subsequent liquid phase sintering. J Alloys Compd. 2021; 865: 158897.
68. Aghaali V, Ebadzadeh T, Zahraee SM, Mirkazemi SM. Microstructure and mechanical properties of WC–TiC–Co cemented carbides produced by spark plasma sintering (SPS) method. SN Appl Sci. 2023; 5: 285.
69. Chen Z, Zhang L, Wu M, Chen C, Zhang Y, Liu J. Pulsed magnetic field treatment of WC-TiC-Co cutting inserts for improved microstructure and cutting performance. J Mater Eng Perform. 2024. doi: 10.1007/s11665-024-09704-z.
70. Barbakadze N, Sarajishvili K, Chedia R, Chkhartishvili L, Tsagareishvili O, Mikeladze A, et al. Obtaining ultrafine powders of some boron carbide-based nanocomposites using liquid precursors. Nanotechnol Percept. 2019; 15: 243-256.
71. Chkhartishvili L, Mikeladze A, Chedia R, Tsagareishvili O, Barbakadze N, Sarajishvili K, et al. Synthesizing fine-grained powders of complex compositions B_4C–TiB_2–WC–Co. Solid State Sci. 2020; 108: 106439.
72. Chkhartishvili L, Mikeladze A, Jalabadze N, Nadaraia L, Korkia T, Chedia R. New low-temperature method of synthesis of boron carbide matrix ceramics ultra-dispersive powders and their spark plasma sintering. Solid State Phenom. 2022; 331: 173-184.
73. Barbakadze N, Chkhartishvili L, Mikeladze A, Tsagareishvili O, Sarajishvili K, Korkia T, et al. Method of obtaining multicomponent fine-grained powders for boron carbide matrix ceramics production. Mater Today Proc 2022; 51: 1863-1871.

74. Chkhartishvili L, Mikeladze A, Chedia R, Tsagareishvili O, Bugdayci M, Karagoz I, et al. Combustion synthesis of boron carbide matrix for superhard nanocomposites production. Adv Combust Synth Technol. 2022; 1: 66-95.
75. Chkhartishvili L, Mikeladze A, Tsagareishvili O, Kvatchadze V, Tavkhelidze V, Mestvirishvili Z, et al. Advanced boron carbide matrix nanocomposites obtained from liquid-charge: Focused review. Condens Matter. 2023; 8: 37.
76. Ozer SC, Buyuk B, Tugrul AB, Turan S, Yucel O, Goller G, et al. Gamma and neutron shielding behavior of spark plasma sintered boron carbide-tungsten based composites. In: TMS 2016 145 th Annual Meeting & Exhibition: Supplemental Proceedings. Cham: Springer International Publishing; 2016. pp. 449-456.
77. Zhang W, Yamashita S, Kita H. Progress in pressureless sintering of boron carbide ceramics–A review. Appl Ceram. 2019; 118: 222-239.
78. Sugiyama S, Taimatsu H. Preparation of WC-WB-W_2B composites from B_4C-W-WC powders and their mechanical properties. Mater Trans. 2002; 43: 1197-1201.
79. Chkhartishvili L, Chedia R, Tsagareishvili O, Mirzayev M, Makatsaria S, Gogolidze N, et al. Preparation of neutron-capturing boron-containing nanosystems. Proceedings of the 9th International Conference & Exhibition on Advanced and Nano Materials; 2022 August 8-10; Victoria, Canada. Ottawa: International Academy of Energy, Minerals and Materials.
80. Chkhartishvili L, Makatsaria S, Gogolidze N. Boron-containing fine-dispersive composites for neutron-therapy and neutron-shielding. In: Proc Int Sci Prac Conf “Innovations and Modern Challenges–2022”. Tbilisi, Georgia: Georgian Technical University; 2023. pp. 221-226.
81. Nabakhtiani G, Chkhartishvili L, Gigineishvili A, Tsagareishvili O, Gabunia D, Rostomashvili Z, et al. Attenuation of gamma-radiation concomitant neutron-absorption in boron-tungsten composite shields. Nano Stud. 2013; 8: 259-266.
82. Evans BR, Lian J, Ji W. Evaluation of shielding performance for newly developed composite materials. Ann Nucl Energy. 2018; 116: 1-9.
83. Chkhartishvili L. Boron-containing nanostructured materials for neutron-shields. In: Nanostructured Materials for the Detection of CBRN. Dordrecht: Springer; 2018. pp. 133-154.
84. Dai M, Zhang Z, Zhu J, Wang X, Xu J, Fu X, et al. Influence of interface roughness on reflectivity of tungsten/boron-carbide multilayers with variable bi-layer number by X-ray reflection and diffuse scattering. Chin Opt Lett. 2009; 7: 738-740.
85. Yeh CL, Wang HJ. Preparation of tungsten borides by combustion synthesis involving borothermic reduction of WO_3. Ceram Int. 2011; 37: 2597-2601.
86. Ozer SC, Turan S, Sahin FC. Mechanical and microstructural properties of spark plasma sintered B_4C–W_2B_5 composites. Proceedings of the 18th International Metallurgy and Materials Congress; 2016 September 29-Ocyober 1; Istanbul, Turkey. Ankara: TMMOB Metalurji ve Malzeme Mühendisleri Odası.
87. Panov VS, Chuvilin AM. Technology and properties of sintered alloys and products made from them (Higher Edu. Inst. Textbook) [Internet]. Moscow: Moscow Institute of Steel and Alloys; 2001. Available from: http://www.materialscience.ru/subjects/materialovedenie/knigi/tehnologiya_i_svoystva_spechennih_tverdih_splavov_i_izdeliy_iz_nih_uchebnoe_posobie_dlya_vuzov__panov_vs_chuvilin_am__m_misis_2001__432_s_07_02_2010/.

88. Shapoval AA, Dragobetskii VV, Savchenko IV. Analysis of processes of shock-wave regeneration of solid alloys [Internet]. National Technical University "Kharkiv Polytechnic Institute"; 2018. Available from: https://repository.kpi.kharkov.ua/server/api/core/bitstreams/5436c07a-afac-4872-9e30-6f31ed9b2740/content.
89. Gachechiladze A, Kandelaki A, Mikadze O, Mikeladze A, Rukhadze L, Jalabadze N, et al. Method for Reception of Nanocrystalline Solid Materials on the Basis of Tungsten Carbide. Tbilisi, Georgia: National Intellectual Property Center of Georgia "GeoPatent"; 2011; Patent Invention P 2011 5141 B. Available from: https://www.sakpatenti.gov.ge/en/publications/?subject=OFFICIALBULLETINSOFINDUSTRIALPROPERTY.
90. Gunjishima I, Akashi T, Goto T. Characterization of directionally solidified B_4C-TiB_2 composites prepared by a floating zone method. Mater Trans. 2002; 43: 712-720.
91. Tsagareishvili O, Mikeladze A, Chedia R, Chkhartishvili L. Method to receive nanostructured solid materials on boron carbide basis. Tbilisi, Georgia: National Intellectual Property Center of Georgia "GeoPatent"; 2018; Patent for Invention P 2018 6907 B. Available from: https://www.sakpatenti.gov.ge/en/publications/?subject=OFFICIALBULLETINSOFINDUSTRIALPROPERTY.
92. Bulut A, Karagöz S. Pyrolysis of table sugar. Sci World J. 2013; 2013: 172039.
93. Ma K, Cao X, Yang H, Xue X. Formation of metastable tungsten tetraboride by reactive hot-pressing. Ceram Int. 2017; 43: 8551-8555.
94. Chkhartishvili L, Mikeladze A, Tsagareishvili O, Barbakadze N, Sarajishvili K, Gabunia V, et al. Effect of cobalt additive on phases formation in boron carbide matrix composites B_4C–$(Ti, Zr)B_2$–W_2B_5. Solid State Sci. 2023; 145: 107339.